JOURNAL OF NATURAL PRODUCTS

pubs.acs.org/jnp

Article

Biosynthesis, Chemical Synthesis, and Pharmacological Evaluation of Lyngbyapeptin A as a GPCR Antagonist of Motilin, Cannabinoid, and Amylin Receptors

Tam H. D. Pham, Manyun Chen, Jie Liu, Qi-Yin Chen, Gustavo Seabra, Valerie J. Paul, Mohamed S. Donia, Steven D. Bruner, Yousong Ding, and Hendrik Luesch*

Cite This: *J. Nat. Prod.* 2025, 88, 2610−2624

Read Online

ACCESS | Metrics & More | Article Recommendations | Supporting Information

ABSTRACT: Lyngbyapeptin A (**1**) is a linear modified tetrapeptide originally isolated from the marine cyanobacterium *Moorena bouillonii* in Papua New Guinea and Guam. In previous research, **1** did not show significant cytotoxicity but was not rigorously investigated due to insufficient material and the propensity of the (*E*)-3-methoxy-2-butenoyl moiety to undergo conversion into a ketone, preventing further biological testing. In this study, we report the identification and characterization of the biosynthetic gene cluster (BGC) of **1** from a *Moorena* collection. The first total synthesis of **1**, of its keto analogue named 5-desmethyl-lyngbyapeptin A (**2**), and of acrylamide analogue **3** was also achieved by convergent liquid-phase peptide synthesis. Compounds **1**−**3** were subjected to functional GPCR target-based *β*-arrestin screens to identify their activity profiles. Four GPCRs, including amylin receptor 2 (CALCR-RAMP2), motilin receptor (MLNR), and cannabinoid receptors CNR1 and CNR2, were antagonized by **1**, supported by secondary functional and binding assays. These receptors were also modulated by **2** and **3** but to a lesser extent, with 2- to 12-fold decrease in potency, demonstrating the role of the (*E*)-3-methoxy-2-butenoyl moiety in contributing to the GPCR modulating activity. The binding modes of **1** to the GPCR hits were further investigated using molecular modeling.

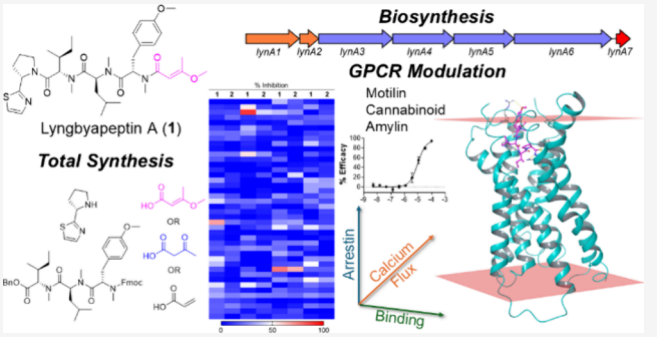

G-protein coupled receptors (GPCRs) represent the largest protein family located on the cell membrane and regulate a broad range of physiological processes in metabolism, neurotransmission, immune responses, and homeostasis.[1] Over the past decades, they have emerged as the most promising targets for new drug discovery with 36% of Food and Drug Administration (FDA)-approved drugs known to target GPCRs.[2] The activation of GPCRs may facilitate different signaling cascades mediated by either the activation of G proteins or the recruitment of *β*-arrestins,[1,3,4] and GPCR modulation at the functional level can be assessed by measuring cytosolic levels of second messengers such as cyclic adenosine 3,5-monophosphate (cAMP), calcium ions,[3−7] or detection of *β*-arrestin recruitment to the receptor.[4,8,9]

Marine cyanobacteria are a group of photosynthetic Gram-negative bacteria, which have been recognized as a valuable source of many structurally diverse specialized metabolites with broad spectrum of biological activities.[10−13] Important groups of these metabolites are ribosomally or nonribosomally synthesized peptides, polyketides, and peptide-polyketide hybrids. There is a growing number of peptidic natural products from marine cyanobacteria acting as GPCR ligands with diverse pharmacological profiles.[14,15] Notable examples include a group of modified linear peptides brintonamides C-E as selective CXCR7 agonists and CCR10 antagonists,[16] the linear peptide amantamide which was identified as a selective CXCR7 agonist,[17] and the macrocyclic tumonolide, a selective TACR2 antagonist.[18]

Lyngbyapeptin A (**1**) is a linear modified tetrapeptide which was first discovered from the marine cyanobacterium *Moorena bouillonii* collected in Papua New Guinea.[19] It was also isolated from collections of the same species found in Guam.[20] Its unique structural features include a terminal (*E*)-3-methoxy-2-butenoyl (Mba) moiety, a proline-derived thiazole-pyrrolidine moiety, and a high level of *N*-methylation. All of these features are also found in other lyngbyapeptins[21−23] (Figure 1). Recently, the biosynthetic gene cluster (BGC) of lyngbyapeptin B, distinguished from lyngbyapeptin A at three amino

Received: August 4, 2025
Revised: September 28, 2025
Accepted: October 2, 2025
Published: October 17, 2025

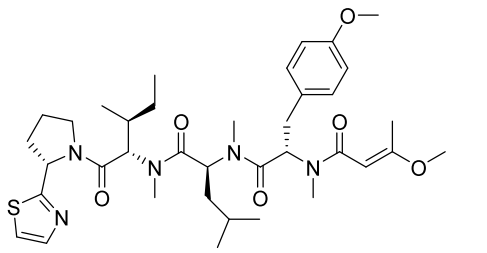

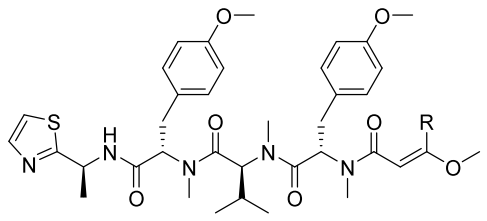

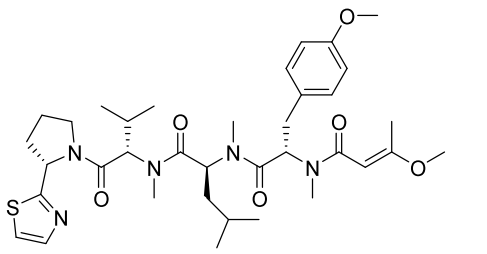

Figure 1. Structures of lyngbyapeptin A (**1**) and other lyngbyapeptins.

acid building blocks (Val-Tyr-Ala sequence in lyngbyapeptin B compared to Leu-Ile-Pro in **1**, see Figure 1), has been identified using genome sequence analysis on *Moorena bouillonii*.[24] The enzymatic logics for the formation of the (*E*)-3-methoxy-2-butenoyl moiety and the C-terminal thiazole moiety were characterized along with the general nonribosomal peptide synthetase (NRPS) and polyketide synthase (PKS) domains, revealing the unique biosynthesis of the hybrid polyketide-nonribosomal peptide structures found in the lyngbyapeptin family.[24] In previous research, **1** did not show significant cytotoxicity against KB and LoVo cancer cells (IC_{50} > 5 μg/mL) but was not rigorously evaluated due to limited isolation amount. Furthermore, it decomposed due to the unstable nature of the (*E*)-3-methoxy-2-butenoyl moiety, preventing further biological testing.[20,22]

In this study, we identified the biosynthetic gene cluster (BGC) of lyngbyapeptin A (**1**) using genomic sequencing and bioinformatic analysis, supported by biochemical studies. Due to the supply and stability challenges, we achieved the first total synthesis of **1** and conducted its pharmacological profiling. As GPCR-targeting marine natural products from cyanobacteria with differential selectivity profiles are emerging,[15] we explored the GPCR targeting potential of **1** and investigated the role of the (*E*)-3-methoxy-2-butenoyl moiety in contributing to its bioactivity by comparing with 5-desmethyl-lyngbyapeptin A (**2**), an analogue of **1** resulting from *O*-demethylation and subsequent enol−keto tautomerization. Acrylamide analogue **3** was later synthesized to probe potential reactive cysteine residues for covalent interaction by increasing the reactivity of the α,β-unsaturated carbonyl system for 1,4-conjugate addition. Our work solved the supply issue and established a synthetic strategy for future preparation of other lyngbyapeptins. It also provided insights into the pharmacological profile and initial structure−activity relationship (SAR) at the GPCR functional level, identifying **1** as an antagonist of the motilin receptor (MLNR), cannabinoid receptor type 1 (CNR1) and 2 (CNR2), and amylin receptor 2 (AMY_2, CALCR-RAMP2) below 20 μM.

RESULTS AND DISCUSSION

Biosynthesis. To elucidate the biosynthetic pathway of lyngbyapeptin A (**1**), we sequenced the genome of VPG18-100, a field collection of *Moorena bouillonii*, which is a lyngbyapeptin A and apratoxins-producing cyanobacterium collected at Finger's Reef, Apra Harbor, Guam.[25,26] Lyngbyapeptin A (**1**) production was confirmed by dereplication, isolation, and NMR analysis (Figure S11). Metagenome sequencing was carried out using the PacBio SEQUEL IIe platform. Subsequent genome assembly yielded 3603 contigs with the largest contig over 3 Mb in length (Table S1). Genome mining of these contigs revealed a putative lyngbyapeptin A BGC (the *lynA* BGC, GenBank accession: PV754024). The 30.2-kb *lynA* BGC shares high similarity to the reported lyngbyapeptin B (*lynB*) BGC (GenBank accession: LC514336[24]), encoding two PKSs (LynA1 and LynA2), four NRPSs (LynA3, LynA4, LynA5, and LynA6), and one nonheme diiron oxygenase (LynA7). The *lynA* PKSs are almost identical to the corresponding proteins encoded in the *lynB* BGC, carrying six domains in the order of GCN5-related *N*-acetyltransferase (GNAT), thiolation (T), ketosynthase (KS), acyltransferase (AT), *O*-methyltransferase (OMT), and thiolation (T) domain (Figure 2A, Table S2). LynA1 is proposed to interact with LynA2 and yield acetoacetyl-LynA2-T, and subsequent *O*-methylation catalyzed by the LynA2-OMT domain generates the (*E*)-3-methoxy-2-butenoyl moiety (Figure 2B), which is supported by the previous report of the *in vitro* biochemical characterization of recombinant LynB2-OMT.[24] According to the NRPS adenylation (A) domain specificity-conferring code,[27,28] the five A domains in the NRPS LynA3-6 are predicted to activate L-Tyr, L-Leu, L-Ile, L-Pro, and L-Cys, respectively (Table S3), which agrees well with the lyngbyapeptin A structure (Figure 1). LynA3 contains two methyltransferase domains while LynA4 and A5 contain embedded NMT domains, resulting in the formation of the *N*,*O*-diMe-L-Tyr-*N*-Me-L-Leu-*N*-Me-L-Ile moiety (Figure 2B). After the incorporation of the last two amino acid building blocks L-Pro and L-Cys by LynA6, the cyclization (Cy) domain converts the *C*-terminal Cys building block into thiazoline and the LynA6 thioesterase (TE) domain then releases the peptide intermediate through hydrolysis (Figure 2B). Identical to the nonheme diiron oxygenase LynB7, LynA7 then generates the final product lyngbyapeptin A by catalyzing the oxidative decarboxylation of 2-thiazoline-4-carboxylic acid to yield 2-thiazole.[24] Given that the key structural difference between lyngbyapeptin A and B (Figure 1) lies in the three amino acid building blocks (Leu-Ile-Pro vs. Val-Tyr-Ala), we further validated the *lynA* BGC by characterizing the substrate specificity of the corresponding A domains. The recombinant A domains from LynA4, LynA5, and the first NRPS module of LynA6 were heterologously expressed in *E. coli* and purified for bioactivity assay (Figure S1). We determined the substrate specificity of these three A domains against selected amino

https://doi.org/10.1021/acs.jnatprod.5c00963
J. Nat. Prod. 2025, 88, 2610−2624

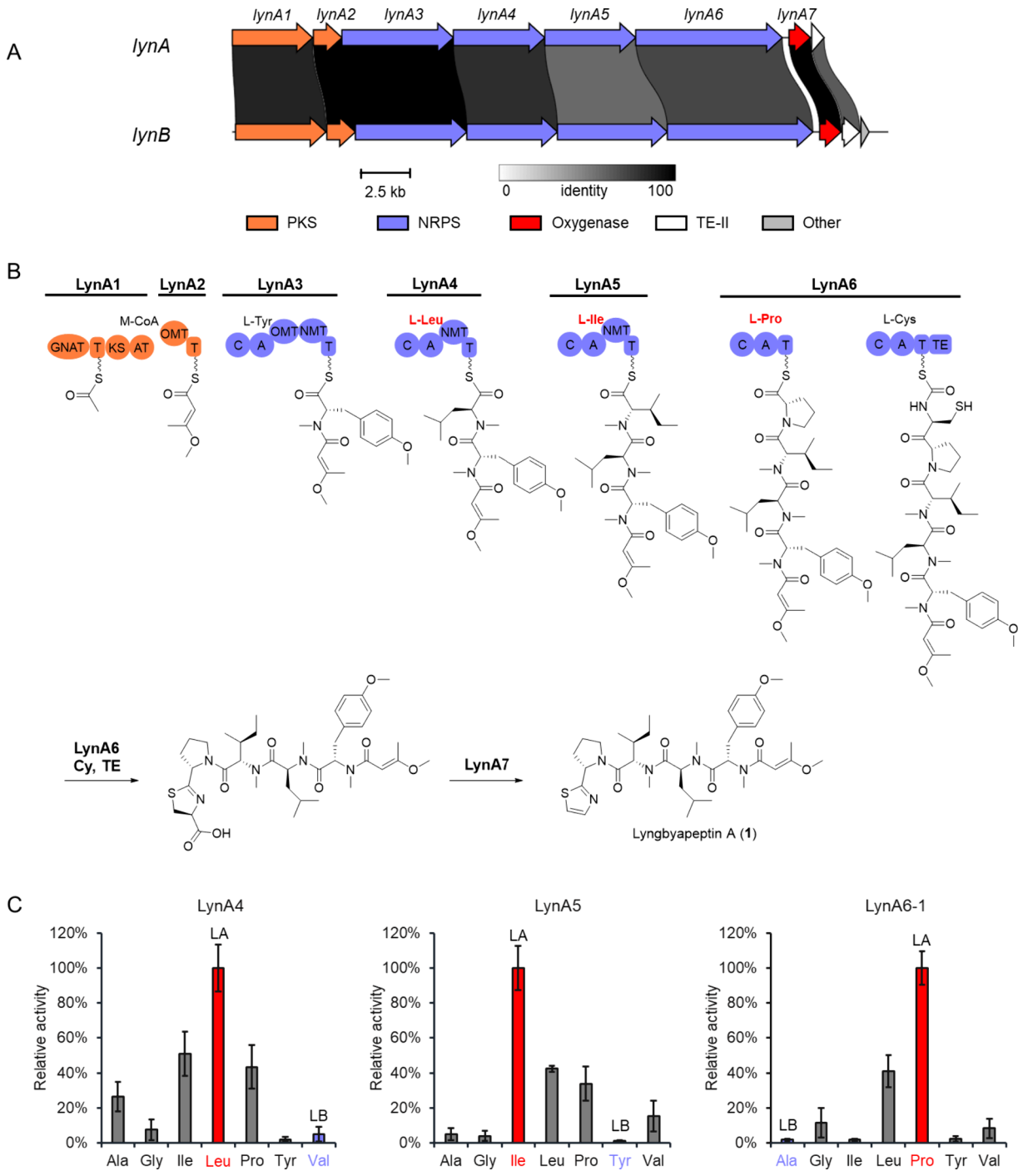

Figure 2. Lyngbyapeptin A (**1**) biosynthetic gene cluster. (A) Comparison of *lynA* with the published *lynB* BGC.[24] The biosynthetic genes with >30% sequence identity were identified by the black-to-white shades according to their sequence identities. PKS: polyketide synthase; NRPS: nonribosomal peptide synthetase; TE-II: type II thioesterase. (B) Proposed biosynthetic pathway of lyngbyapeptin A. The predicted *lynA* amino acid building blocks that are different from those in the corresponding positions in *lynB* are highlighted in red. M-CoA: malonyl-CoA; GNAT: GCN5-related *N*-acetyltransferase; T: thiolation; KS: ketosynthase; AT: acyltransferase; MT: *N*- or *O*-methyltransferase; C: condensation; A: adenylation; TE: thioesterase. (C) Relative activity of different amino acids activated by recombinant A domains of LynA4, LynA5, and LynA6-1. LA: the native substrates in lyngbyapeptin A; LB: the native substrates in lyngbyapeptin B. Ala: alanine; Gly: glycine; Ile: isoleucine; Leu: leucine; Pro: proline; Tyr: tyrosine; Val: valine. The data represent means ± s.d. of four independent experiments.

acids, including LynB substrates, by the hydroxylamine assay.[29] As expected, the recombinant LynA4, LynA5, and LynA6-1 A domains showed the highest activity toward L-Leu, L-Ile, and L-Pro, respectively, supporting their role in the lyngbyapeptin A biosynthesis (Figure 2C). Taken together, this work identified and validated the *lynA* BGC through bioinformatic analysis and biochemical studies and highlighted the distinction from the *lynB* BGC.

Chemical Synthesis. The retrosynthetic analysis of lyngbyapeptin A (**1**) and its two analogues, 5-desmethyl-lyngbyapeptin A (**2**) and acrylamide analogue **3**, is shown in Figure 3. All compounds share the common fragment

https://doi.org/10.1021/acs.jnatprod.5c00963
J. Nat. Prod. 2025, 88, 2610−2624

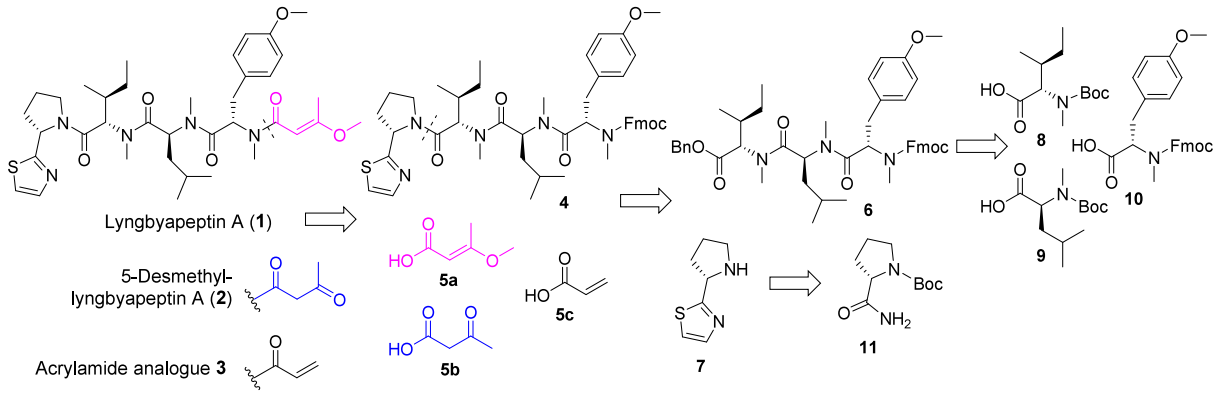

Figure 3. Retrosynthetic analysis of lyngbyapeptin A (**1**), 5-desmethyl-lyngbyapeptin A (**2**), and acrylamide analogue **3**.

Scheme 1. Total Synthesis of Lyngbyapeptin A (1), 5-Desmethyl-lyngbyapeptin A (2), and Acrylamide Analogue 3[a]

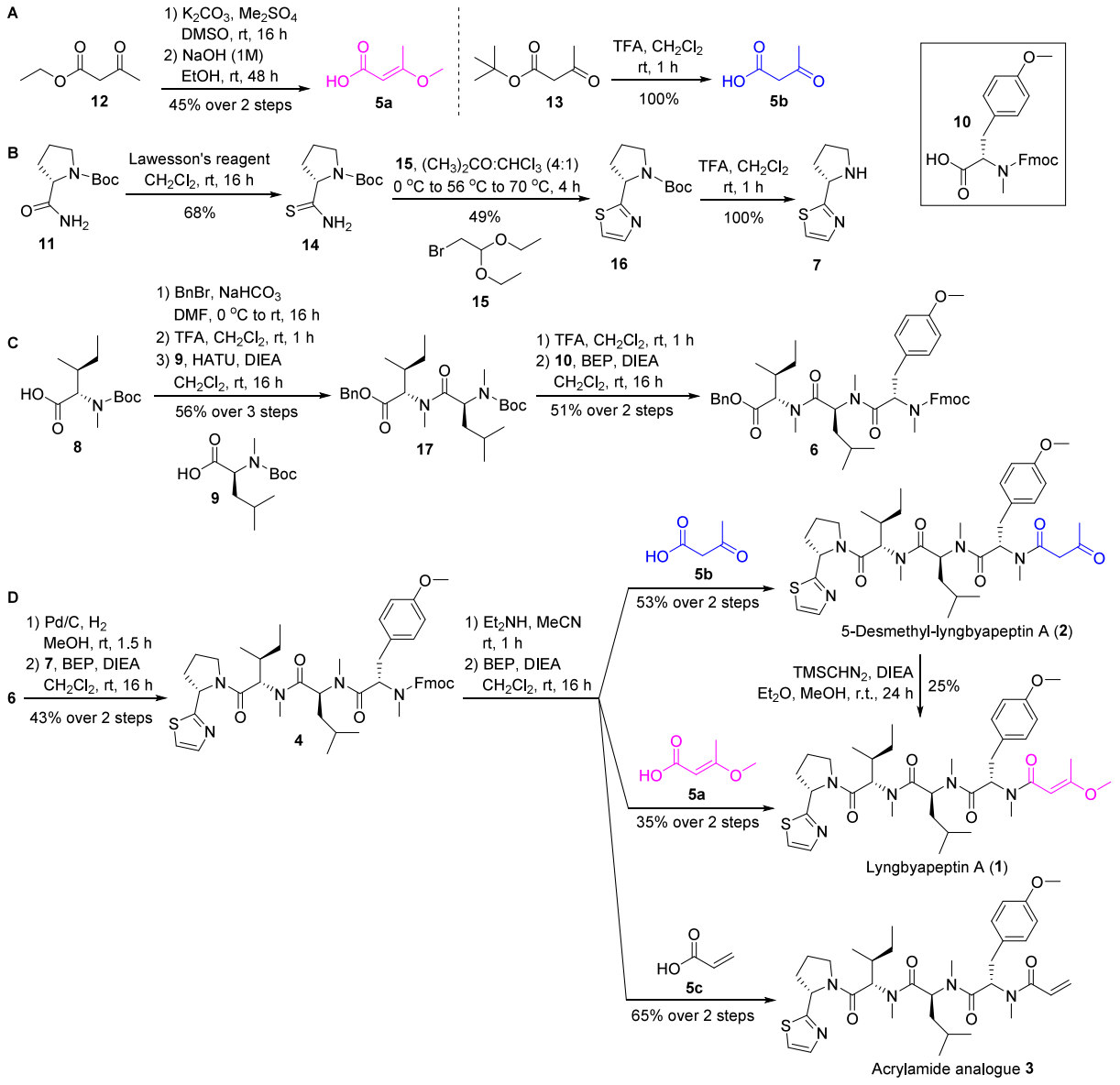

[a](A) Synthesis of methyl enol ether **5a** and acetoacetic acid **5b**. (B) Synthesis of thiazole **7**. (C) Synthesis of tripeptide **6**. (D) Synthesis of tetrapeptide **4** and **1**−**3**. HATU: *O*-(7-azabenzotriazole-1-yl)-1,1,3,3-tetramethyluronium hexafluorophosphate; DIEA: *N*,*N*-diisopropylethylamine; BEP: 2-bromo-1-ethyl-pyridinium tetrafluoroborate; $TMSCHN_2$: trimethylsilyldiazomethane.

https://doi.org/10.1021/acs.jnatprod.5c00963
J. Nat. Prod. 2025, 88, 2610−2624

tetrapeptide **4**. We envisioned the late-stage installation of the two terminal moieties, thiazole pyrrolidine **7** and methyl enol ether **5a**, to minimize conversion of unstable **1** to **2** via demethylation and tautomerization. Tripeptide **6** could be synthesized via sequential condensation of *N*-methylated amino acids. Methyl enol ether **5a**, acetoacetic acid **5b**, and thiazole **7** could be synthesized from commercially available starting materials as previously reported[24,30−32] (Figure 3).

Based on the method established by Hanquet et al.,[30] the synthesis of methyl enol ether **5a** started from the methylation of commercially available ethyl acetoacetate **12** to afford (*E*)-ethyl-3-methoxy-2-butenoate, followed by hydrolysis with aqueous NaOH in EtOH provided the desired **5a**[24] in 50% yield (Scheme 1A). Acetoacetic acid **5b** was prepared from acidic cleavage of the *tert*-butoxide group from the commercially available *tert*-butyl acetoacetate **13** using TFA in CH_2Cl_2.

Thiazole pyrrolidine **7** was derived from the commercially available Boc-L-proline amide **11** by employing a modified Hantzsch thiazole formation reaction (Scheme 1B). Conversion of amide **11** to thioamide **14** was achieved by using Lawesson's reagent in CH_2Cl_2 at room temperature in 68% yield. However, condensation of **14** with 2-bromoacetaldehyde diethyl acetal **15** in THF at reflux did not provide the desired thiazole **16** as in the reported protocols[31,32] despite several attempts. Through screening of various solvent systems, a mixture of acetone and $CHCl_3$ (4:1 ratio *v*/*v*) was the most optimal condition for the reaction and furnished **16** in 49% yield. We hypothesized that the acidity of $CHCl_3$ converts the acetal to the corresponding aldehyde, thereby promoting the reaction more efficiently. Boc deprotection of thiazole **16** readily furnished thiazole **7** in quantitative yield.

As depicted in Scheme 1C, the synthesis of tripeptide **6** started from converting Boc-*N*-methyl-L-isoleucine **8** to its corresponding benzyl ester followed by removal of the Boc group using TFA. The free amine was then coupled with Boc-*N*-methyl-L-leucine **9** using *O*-(7-azabenzotriazole-1-yl)-1,1,3,3-tetramethyluronium hexafluorophosphate (HATU) as the coupling reagent to yield dipeptide **17**. After acidic cleavage of the Boc group from **17** by treatment with TFA, the corresponding amine was coupled with Fmoc-*N*,*O*-dimethyl-L-tyrosine (**10**) in the presence of HATU and *N*,*N*-diisopropylethylamine (DIEA) to afford tripeptide **6** in only 16% yield due to epimerization. To optimize the reaction, two other coupling reagents were screened: *N*,*N*′-bis(2-oxo-3-oxazolidinyl)phosphinic chloride (BOP-Cl) and 2-bromo-1-ethyl-pyridinium tetrafluoroborate (BEP), which have been reported as being suitable for coupling substrates with steric hindrance and *N*-methylated amino acids.[33] While BOP-Cl resulted in low solubility in CH_2Cl_2 and the starting material was recovered, BEP furnished the best result with 51% yield of tripeptide **6** (Table 1; entries 1−3).

The synthesis of tetrapeptide **4** started from the hydrogenolytic debenzylation of tripeptide **6** using Pd/C in MeOH followed by the coupling of the corresponding acid with the thiazole pyrrolidine **7** (Scheme 1D). Similar to the synthesis of tripeptide **6**, various coupling reagents were screened to maximize the yield. HATU, BOP-Cl, and [(7-azabenzotriazol-1-yl)oxy]tris(pyrrolidino)phosphonium hexafluorophosphate (PyAOP) afforded no desired product while BEP was able to provide tetrapeptide **4** in 43% yield (Table 1; entries 4−7).

Due to the unstable nature of 5-desmethyl-lyngbyapeptin A (**2**), we first explored the optimal conditions for its synthesis

Table 1. Screening of Coupling Reagents for Amide Bond Formation to Form Tripeptide 6 (Entries 1−3) and Tetrapeptide 4 (Entries 4−7)

Entry	Coupling reaction	Coupling reagent	Yield (%)
1	**17** + **10** → **6**	HATU	16
2	**17** + **10** → **6**	BOP-Cl	0
3	**17** + **10** → **6**	BEP	51
4	**6** + **7** → **4**	HATU	0
5	**6** + **7** → **4**	BOP-Cl	0
6	**6** + **7** → **4**	PyAOP	0
7	**6** + **7** → **4**	BEP	43

which were also applied in the subsequent synthesis of the natural product lyngbyapeptin A (**1**) and acrylamide analogue **3**. After removal of the Fmoc group using Et_2NH in MeCN, the free amine of tetrapeptide **4** was subjected to the final amide condensation step with acetoacetic acid **5b**. Through screening, BEP was the coupling reagent of choice to facilitate the coupling between the free amine and **5b** to afford **2** with 53% yield, while the use of HATU, PyAOP, and benzotriazol-1-yloxytri(pyrrolidino)phosphonium hexafluorophosphate (PyBOP) did not yield the desired product. The free amine of **4** was also subjected to coupling reaction with commercially available acrylic acid **5c** using BEP to furnish acrylamide analogue **3** in 65% yield.

With compound **2** in hand, we first attempted the conversion of its 1,3-butanedione unit to (*E*)-3-methoxy-2-butenoyl unit in lyngbyapeptin A (**1**) via a reverse tautomerization and methylation using trimethylsilyldiazomethane ($TMSCHN_2$).[34] However, the reaction often resulted in low yield (25%) and the unreacted **2** suffered from epimerization after recovery of the starting material. We also attempted to optimize the methylation step with other synthetic strategies such as dimethyl sulfate under basic condition, trimethyl orthoformate with sulfuric acid, or Lewis acid catalyst montmorillonite. However, they were ineffective and resulted in no reaction or decomposition of compound **2** due to the harsh acidic or basic conditions used. Therefore, similarly to the synthesis of compound **2**, we applied a synthetic strategy in which the methyl enol ether **5a** was synthesized according to published reports (Scheme 1A) and coupled to the free amine of tetrapeptide **4** as the final step to obtain the final product **1** in 35% yield over two steps.

Compared with isolated lyngbyapeptin A (**1**),[19,20] our synthetic sample showed identical ^1H and ^{13}C NMR spectra and comparable optical rotation value ($[\alpha]^{26}_D$ −258 (*c* 0.58, MeOH), lit. $[\alpha]^{25}_D$ −235 (*c* 0.58, MeOH)),[20] validating the structural assignment.

Bioactivity. Because of previous findings that cyanobacterial peptides modulate GPCR activity and with sufficient material in hand, we tested the synthetic compounds for their ability to modulate GPCRs. Compounds **1** and **2** were profiled against a panel of 168 GPCR targets in both agonist and antagonist mode at 20 μM final concentration in a cell-based functional screen using PathHunter β-arrestin assay technology (Figure 4A). Comparison of both profiles would provide the biological role of the (*E*)-3-methoxy-2-butenoyl moiety present in the natural product. While both compounds had no agonistic effect on any of the tested targets, **1** modulated cannabinoid receptor CNR2, motilin receptor MLNR, amylin receptor 2 CALCR-RAMP2, and cannabinoid receptor CNR1 activity with 89, 76, 68, and 53% inhibition, respectively

https://doi.org/10.1021/acs.jnatprod.5c00963
J. Nat. Prod. 2025, 88, 2610−2624

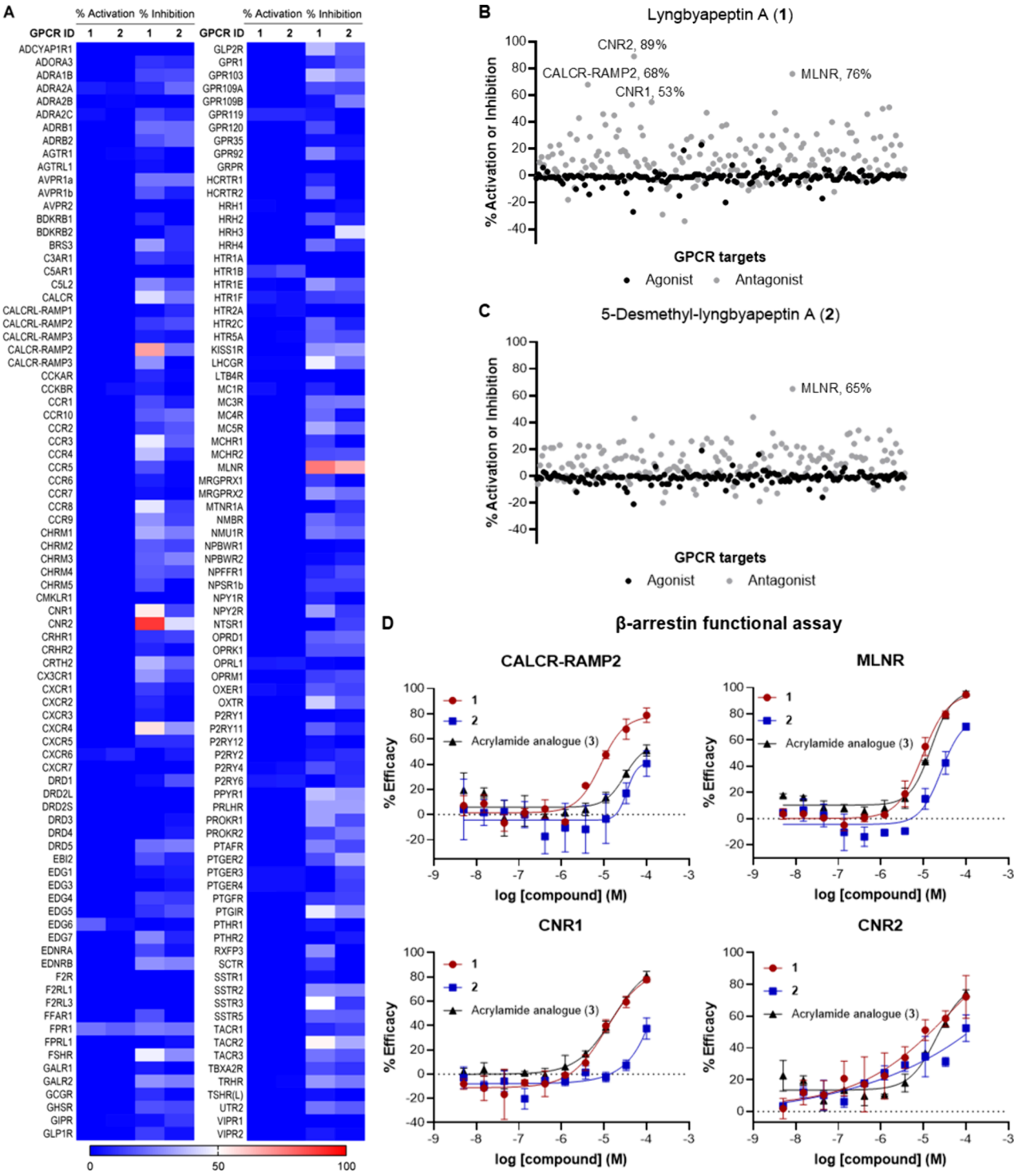

Figure 4. GPCR profiling of lyngbyapeptin A (**1**) and 5-desmethyl-lyngbyapeptin A (**2**) using cell-based functional β-arrestin screen. (A) Heatmap showing the profiling data of **1** and **2** against the gpcrMAX panels of 168 GPCR targets. (B, C) Scatter plots showing the % activation or inhibition of **1** and **2** at 20 μM against the gpcrMAX panel (agonist and antagonist modes). The hits identified in the screen with >50% activity or inhibition are labeled. (D) Dose−response curves for **1**−**2** and acrylamide analogue **3** in antagonist mode against confirmed hits: CALCR-RAMP2, CNR1, CNR2, and MLNR. Calcitonin (IC_{50} 0.047 μM), CP55940 (IC_{50} 0.019 μM), CP55940 (IC_{50} 0.013 μM), and motilin (IC_{50} 0.014 μM) were the ligands used as positive controls for CALCR-RAMP2, CNR1, CNR2, and MLNR, respectively. Data are presented as mean ± SD (n = 2).

(Figure 4B). MLNR was the only target of **2** with 65% inhibition (Figure 4C) in the antagonist mode. Compared to the GPCR hit CALCR-RAMP2, **1** only inhibited 43% of calcitonin receptor CACLR and 29% of amylin receptor 3 CALCR-RAMP3 in the antagonist mode. Hence, they were not selected for subsequent target validation assays but suggested subtle selectivity.

Next, **1** and **2** were tested in a dose−response manner starting at 100 μM, using the same β-arrestin assay to validate the hits identified in the primary screen (Figure 4D, Table 2). Compound **1** exhibited moderate activity against the tested

https://doi.org/10.1021/acs.jnatprod.5c00963
J. Nat. Prod. 2025, 88, 2610−2624

Table 2. IC_{50} Values (μM) for Lyngbyapeptin A (1), 5-Desmethyl-lyngbyapeptin A (2), and Acrylamide Analogue 3 against the GPCR Hits Identified in the Primary β-Arrestin Screen

Compound	CALCR-RAMP2	MLNR	CNR1	CNR2
Lyngbyapeptin A (1)	8.44	9.55	11.6	17.7
5-Desmethyl-lyngbyapeptin A (2)	>100	28.0	>100	36.7
Acrylamide analogue 3	62.6	15.3	16.0	20.8
Selectivity index (1 over 2)	>12-fold	2.9-fold	>8.6-fold	2.1-fold
Selectivity index (1 over 3)	7.4-fold	1.6-fold	1.4-fold	1.2-fold

GPCR targets with IC_{50} values in a low micromolar range, while **2** showed significantly reduced activity against the tested GPCR targets (IC_{50} > 20 μM). In particular, **1** exhibited selective inhibition against CNR1 and CNR2 with approximately 9-fold and 2-fold increase in potency compared to **2**, demonstrating that the (*E*)-3-methoxy-2-butenoyl moiety contributes to the bioactivity and its conversion to the keto version attenuates the activity. We also tested acrylamide analogue **3** against the four GPCR targets identified in the primary screen to probe for potential reactive cysteine residues for covalent interaction, by increasing the reactivity of the α,β-unsaturated carbonyl system for 1,4-conjugate addition. Compared to the natural product, **3** exhibited similar activity except a 7.4-fold decrease in potency against CALCR-RAMP2 (Figure 4D, Table 2). To determine whether the terminal conjugated enol ether in **1** could act as a Michael acceptor and has the potential to covalently modify its pharmacological targets, the compounds were tested in an ARE-luciferase reporter assay which probes for Keap1/Nrf2 pathway activation. The Kelch-like ECH-associated protein 1 (Keap1) is a cysteine-rich protein, which under homeostasis forms a complex with part of an E3 ubiquitin ligase and the nuclear factor E2-related factor 2 (Nrf2), leading to the degradation of this transcription factor by the ubiquitin-proteasome system. When under stress, reactive thiol from cysteine side chains of Keap1 undergoes oxidation by reactive oxygen species (ROS) or alkylation by electrophilic compounds, causing Nrf2 to dissociate from Keap1 and subsequently bind to and activate the antioxidant response element (ARE).[35,36] Compound **3** strongly activated the reporter, showing activation by 3.5-fold at 10 μM and 152-fold at 100 μM, while the natural product **1** and its keto analogue **2** were inactive (Figure S2). Substitution at the β position with two electron-donating groups, as in the terminal enol ether of lyngbyapeptin A (**1**), deactivates the system for a 1,4-addition of nucleophiles. Taken together, the α,β-unsaturated carbonyl in (*E*)-3-methoxy-2-butenoyl moiety in **1** is essential for effective GPCR antagonistic activity but not through covalent modification.

The cannabinoid receptors are among the most abundant members of the GPCR family in humans.[37] Cannabinoid receptor type 1 (CNR1, also known as CB_1) is highly expressed on the central neurons in the brain, and cannabinoid receptor type 2 (CNR2 or CB_2) is present mainly in immune cells and tissues.[38,39] These GPCRs have attracted considerable attention as therapeutic targets for pain, cancer, inflammation-derived neurodegenerative diseases, and osteoporosis.[40] Motilin is an endogenous peptide hormone found in the human gastrointestinal (GI) tract.[41,42] Upon binding to motilin receptors (MLNR or MTLR), the hormone stimulates GI motility and regulates food digestion, hunger signaling, and hormone secretion in the GI tract.[41,42] Motilin and its GPCR have attracted interests in drug development for the treatment of obesity, GI disorders, and diabetes.[41,43] Besides acting by themselves, GPCRs can also interact with accessory proteins, which can modulate receptor phenotype and further diversify GPCR ligands and functions.[44] The receptor activity-modifying protein (RAMP) is a prime example, and its interaction with the calcitonin receptor (CT or CALCR) forms the amylin receptor (AMY) with three subtypes: AMY_1 (CALCR-RAMP1), AMY_2 (CALCR-RAMP2), and AMY_3 (CALCR-RAMP3).[45,46] Amylin is a pancreatic peptide hormone which regulates insulin secretion and glucose metabolism.[45−47] Compared to CT which has high affinity for calcitonin and weak response to amylin when expressed independently of RAMPs,[47] AMYs have higher affinity for amylin and other related peptides with different selectivity upon activation. CALCR-RAMP1 has higher affinity for calcitonin gene-related peptide (CGRP) than amylin and vice versa for CALCR-RAMP3.[45,46] CALCR-RAMP2 complex has not been thoroughly investigated due to its cell-type dependency, which results in variable phenotype, hence its role remains elusive.[44−46]

Similarly to the activity found in the functional β-arrestin dose−response analysis (IC_{50} 9.55 μM, Table 2; Figure 4D), natural product **1** was found to have micromolar binding affinity to MLNR with K_i value of 3.31 μM and IC_{50} of 6.62 μM (Figure 5A). To evaluate **1**'s potential other mode of activity besides β-arrestin signaling pathway, we examined the calcium mobilization in MLNR induced by **1** using Calcium No Wash^{PLUS} assay technology. Upon activation of GPCR by ligand binding, MLNR initiates signal transduction through the release of intracellular calcium, which allows the use of fluorescent calcium dyes to measure transient changes of cytosolic calcium concentration.[42] As shown in Figure 5C, **1** regulated GPCR-mediated calcium signaling in MLNR as an antagonist with an IC_{50} of 8.78 μM, indicating a strong correlation between binding and functional responses across assay systems.

The binding mode of **1** into MLNR was further investigated using molecular modeling of the receptor's cryo-EM structure in complex with the macrolide antibiotic erythromycin, an agonist of MLNR (PDBID: 8IBU) (Figure 5C). Besides erythromycin's therapeutic effects on bacterial infections such as tonsillitis, acute sinusitis, and pneumonia,[48] long-term use of the drug often causes stimulation of the GI motor activity, hence its off-target effect on MLNR.[42,49,50] **1** bound to the same binding pocket as erythromycin, with some additional residue interactions (docking scores: **1** = −4.7, erythromycin = −6.2). MLNR establishes hydrogen bonds (HB) to erythromycin via Arg318 and forms salt bridges with Asp94 and Glu119 (Figure S3). The binding pose obtained shows lyngbyapeptin A (**1**) establishing the same interaction with Arg318 at the thiazole ring, plus two new hydrogen bonds with Arg97, and this pose was used as input for 100 ns MD simulations (Figures 5D,E and S4−6). The hydrogen bond to **1** from Arg318 is maintained for 69% of the time. Glu234 also

https://doi.org/10.1021/acs.jnatprod.5c00963
J. Nat. Prod. 2025, 88, 2610−2624

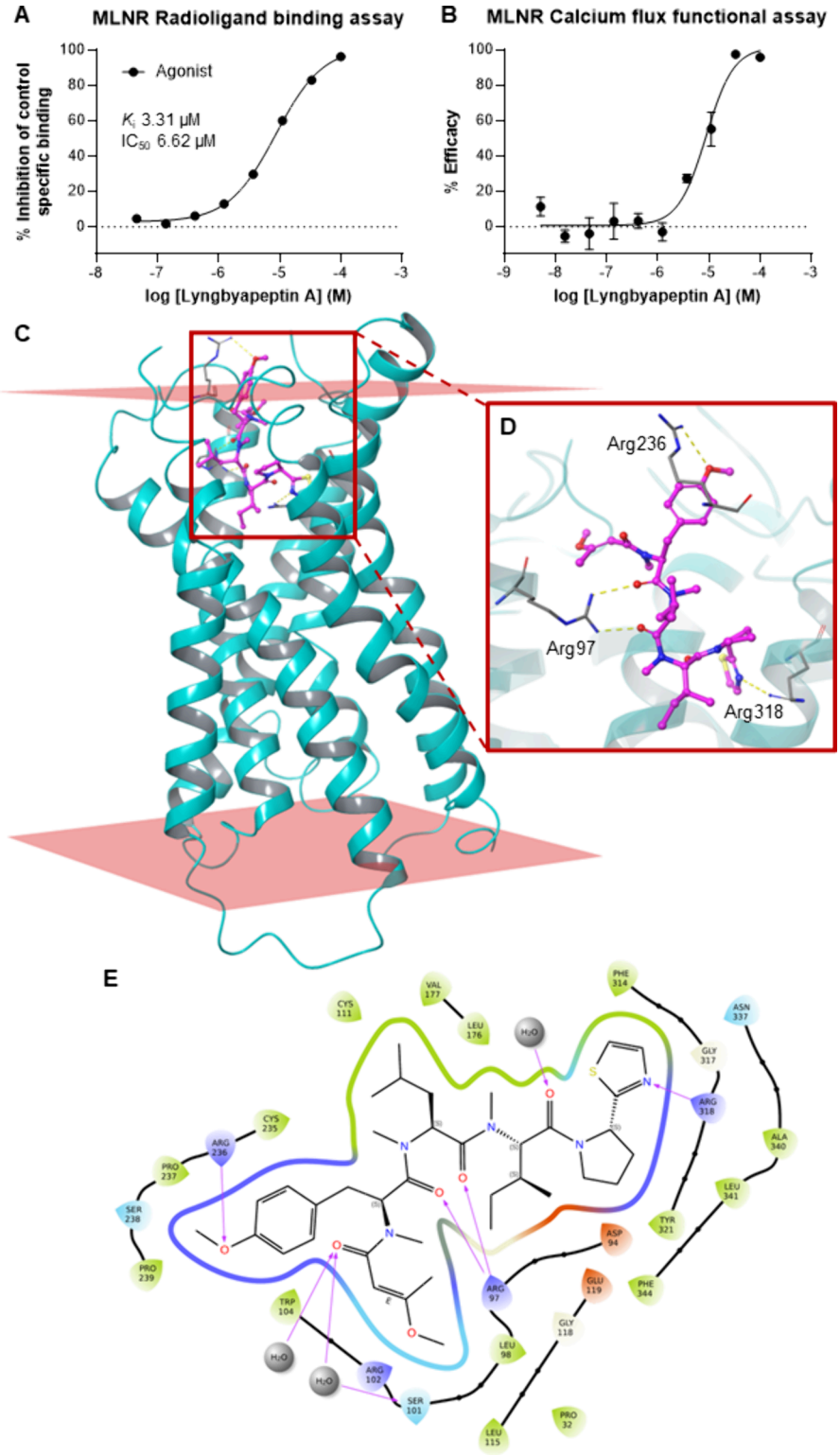

Figure 5. Lyngbyapeptin A (**1**) binding, functional response characterization, and molecular modeling into MLNR. (A) Competitive radioligand binding assay of **1** to MLNR in agonist mode. (B) Effect of **1** in MLNR calcium flux functional assay in antagonist mode. Data are presented as mean ± SD (n = 2). (C) The whole complex of **1** into MLNR from molecular modeling. (D) Docking poses obtained for **1**. (E) Diagram of interactions between **1** and MLNR. Pink arrows indicate hydrogen bonds (donor to acceptor), and gray circles indicate solvent exposure.

interacts with **1** through water bridges 74% of the time. Other important hydrogen bonds are from Arg97 with the carbonyls from the enol ether, Tyr, and Leu residues in **1**, which are present approximately 50% or higher of the time as direct bonds. The hydrogen bond to Asp94 is quickly lost and replaced by hydrophobic interactions with the Leu residue in **1** (Figures S4–6).

We then compared the functional β-arrestin dose–response analysis of **1** against the cannabinoid receptors with binding affinities under different conditions. We tested **1** in competitive

https://doi.org/10.1021/acs.jnatprod.5c00963
J. Nat. Prod. 2025, 88, 2610–2624

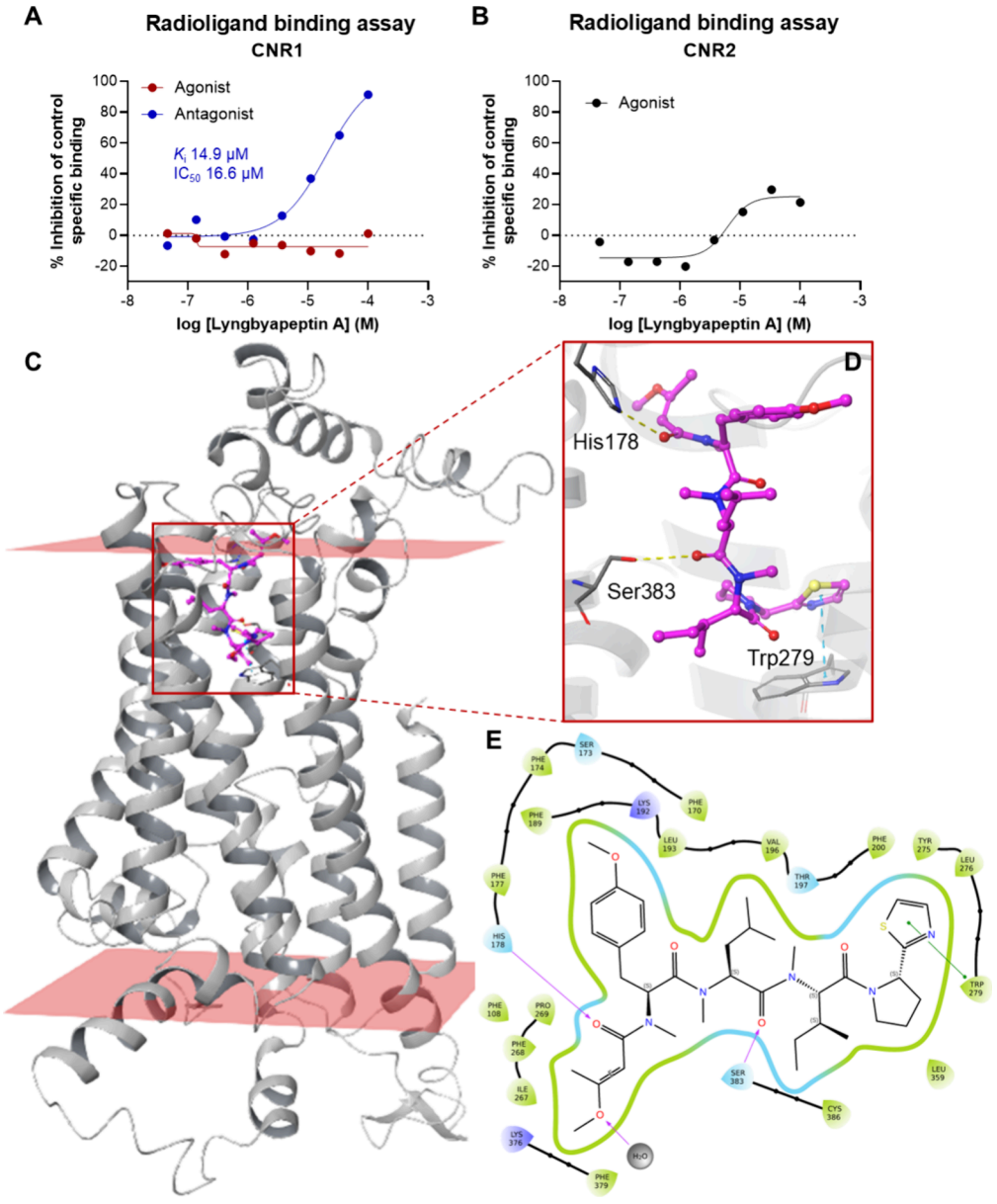

Figure 6. Lyngbyapeptin A (**1**) binding, functional response characterization, and molecular modeling into CNR1 and CNR2. (A) Competitive radioligand binding assay of **1** to CNR1 against agonist (red) or antagonist (blue) radioligand. (B) Competitive radioligand binding assay of **1** to CNR2 against agonist radioligand. All data are presented as mean ± SD (n = 2). (C) The whole complex of **1** into CNR1 from molecular modeling. (D) Docking poses obtained for **1**. (E) Diagram of interactions between **1** and CNR1. Pink arrows indicate hydrogen bonds (donor to acceptor), and gray circles indicate solvent exposure.

radioligand binding assays against human CNR1, which were incubated with either an agonist or antagonist radioligand (Figure 6A). An agonist radioligand labels high-affinity binding sites, while an antagonist radioligand labels both high and low-affinity binding sites, which are in excess compared to the high-affinity binding sites.[51] Testing in both models would allow us to access the natural product's potential binding sites. Binding data suggest that **1** competed with the antagonist radioligand and had a moderate binding affinity to CNR1 (K_i 14.9 μM, IC_{50} 16.6 μM), which correlates with the cellular activity of **1** in the β-arrestin assay (IC_{50} 11.6 μM, Table 2; Figure 4D). We also tested **1** in a competitive radioligand binding assay against human CNR2, which was incubated with an agonist radioligand (Figure 6B). Compound **1** might have competed for high-affinity binding sites in CNR2, in which its K_i and IC_{50} values are 4.0 μM and 6.1 μM, respectively. However, antagonists bind equally to high and low-affinity binding sites, and the agonist radioligand utilized in this CNR2 binding assay only labels high-affinity binding sites.[51] There was no assay readily available for competitive ligand binding with CNR2 against an antagonist radioligand. Therefore, the current results could not fully reflect **1**'s binding to CNR2 as an antagonist.

To gain insights into the binding mode of **1** to CNR1, we performed modeling studies using the crystal structure of CNR1 in complex with AM6538, an analogue of rimonabant and antagonist of CNR1 (PDBID: 5TGZ). From dockings, **1** establishes HB to CNR1 via His178 and Ser383, as well as $\pi-\pi$ stacking with Trp279 at the thiazole ring (Figures 6D and S7). This pose was used as input for 100 ns MD simulations

https://doi.org/10.1021/acs.jnatprod.5c00963
J. Nat. Prod. 2025, 88, 2610−2624

(Figures 6D,E and S7−9). The hydrogen bond to **1** from His178 is maintained 98% of the time. Besides interacting with Trp279 at 75% of the time, the thiazole ring also has $\pi-\pi$ stacking with Phe268 but not as frequently (43%). HB between Thr197 and the carbonyl from the Pro residue is present approximately 50% of the time as a direct bond. The Tyr residue of **1** has two additional interactions: salt bridges between Asp184 and the *O*-methyl at 31% and $\pi-\pi$ stacking with Phe177 at 34% of the time (Figures S7 and S8).

We assessed the viability of transfected HEK293 human embryonic kidney cells upon compound treatment (Figure S10A). Treatment with **1** resulted in 50% viability at 32 μM. **2** had an IC_{50} higher than 100 μM, whereas **3** had an IC_{50} of 58 μM. These findings validate that no cytotoxicity was associated with **1** at its effective concentrations in our GPCR assays. We also evaluated the antiproliferative activity of **1**−**3** against HCT116 colorectal cancer cells (Figure S10B). While **2** and **3** did not show any effects on cell viability up to the highest concentration tested (100 μM), **1** reduced viability by more than 50% only at 100 μM. These data are consistent with the lack of cytotoxicity reported for KB and LoVo cancer cells, where the highest concentration tested was 5 μg/mL, corresponding to an IC_{50} > 7.2 μM.[20]

In summary, we identified and characterized the BGC of the marine cyanobacterial natural product lyngbyapeptin A (**1**) using bioinformatic analysis and biochemical studies. We also achieved the total synthesis of **1** and analogues with an efficient method to minimize decomposition, which can be applied to the synthesis of other lyngbyapeptins. Screening for GPCR-modulating activity of **1** identified CALCR-RAMP2, MLNR, CNR1, and CNR2 as notable hits in the antagonist mode and suggested that the (*E*)-3-methoxy-2-butenoyl moiety contributes to the natural product's GPCR antagonistic activity against CNR1 and MLNR, in particular, and its binding modes with the two targets were further explored in computational studies. Our study provides a platform for the assessment of GPCR-modulating activities of modified peptides from marine cyanobacteria.

EXPERIMENTAL SECTION

General Experimental Procedures. All commercial reagents were used without further purification. Solvents were purified by PS-MD-5 solvent purification system (Innovative Technology Inc., now Inert Corp.). All reactions were performed in heat-gun-dried flasks (400 °C under reduced pressure) under an inert atmosphere of anhydrous argon or nitrogen gas. Thin-layer chromatography was performed on MilliporeSigma silica gel 60 Å F_{254} glass plates. Flash column chromatography was performed with Fisher 170−400 mesh silica gel. HRMS data were obtained using a Q Exactive Focus (Thermo Fisher) with an electrospray ionization (ESI) interface operated in positive and negative modes. NMR spectra were recorded on a Bruker Avance II 600 MHz high-resolution 5 mm cryoprobe spectrometer and a Bruker Avance Neo-600 spectrometer with a broadband Prodigy cryogenic probe. Chemical shifts for ^{1}H NMR spectra are reported in ppm relative to the signal of residual $CDCl_3$ at 7.26 ppm. Chemical shifts for ^{13}C NMR spectra are reported in ppm relative to the center line of the $CDCl_3$ triplet at 77.16 ppm. Optical rotation was measured on a Rudolph Research Analytical Autopol III automatic polarimeter using a microcell of 1 dm path length.

Extraction and Isolation. A field collection of *Moorena bouillonii* (VPG18-100) was made on April 10, 2018 at Fingers Reef, Apra Harbor, Guam. The sample was lyophilized and extracted with EtOAc and MeOH (1:1) to afford a lipophilic extract (383 mg) which was then partitioned between hexanes and 80% aqueous MeOH. The MeOH-H_2O fraction was dried and further partitioned between *n*-BuOH and H_2O. The *n*-BuOH soluble fraction was dried and subjected to silica chromatography using a step gradient system of increasing *i*-PrOH in CH_2Cl_2. Based on ^{1}H NMR and low-resolution MS analysis, the mixture eluting with 4% *i*-PrOH in CH_2Cl_2 (3.29 mg) was further purified by analytical reversed-phase HPLC (column, Phenomenex Synergi 4 μm Hydro-RP 80 Å, 250 × 4.6 mm; flow rate, 1.0 mL/min; PDA detection 190−400 nm) using a MeCN-H_2O linear gradient (35−100% MeCN for 35 min, 100% MeCN for 5 min, and then 100%−35% MeCN for 5 min) to afford lyngbyapeptin A (t_R 24.05 min, 0.36 mg).

Lyngbyapeptin A (1). Colorless amorphous solid; $[\alpha]^{26}_D$ −203 (*c* 0.04, MeOH), lit. $[\alpha]^{25}_D$ −235 (*c* 0.58, MeOH);[20] ^{1}H NMR (Supporting Information, Figure S11); HRMS (ESI) *m*/*z* 720.3755 $[M + Na]^+$ (calcd for $C_{37}H_{55}N_5O_6SNa$, 720.3771).

Genomic DNA Isolation and Metagenome Sequencing of VPG18-100. The metagenomic DNA of *Moorena bouillonii* (VPG18-100) was obtained using the QIAamp DNA Micro Kit (Qiagen) and further purified with the DNeasy PowerClean Pro Cleanup kit (Qiagen). The metagenome sequencing was performed using the PacBio SEQUEL IIe sequencing platform with a SMRT cell at the UF Interdisciplinary Center for Biotechnology Research. The metagenome was assembled by the metaFlye assembler and annotated by AntiSMASH.[52] The putative *lynA* BGC was further analyzed by BLAST homology tool and NRPSpredictor2.[53]

Expression and Purification of LynA4, LynA5, and LynA6 Adenylation (A) Domains. The gene fragments encoding the predicted LynA4, LynA5, and LynA6-1 A domains were synthesized by Twist Biosciences (Table S4). The pET28b vector and the synthesized gene fragments were digested by NdeI and XhoI and then ligated by T4 ligase (Thermo Scientific). The resulting constructs were verified by Sanger sequencing (Genewiz) and transformed into *E. coli* BL21(DE3) cells. For protein expression, overnight cultures were diluted 1:100 in 1 L of LB broth containing 50 μg/mL kanamycin and cultured at 37 °C, 200 rpm until OD600 reached 0.6. The culture was then cultured at 16 °C, 180 rpm for 18 h. The cells were harvested by centrifugation (6000 rpm, 15 min), and collected cell pellets were resuspended in the lysis buffer (25 mM Tris-Cl, pH 8.0, 100 mM NaCl, 1 mM β-mercaptoethanol, and 10 mM imidazole) and lysed by sonication on ice (10 s pulse and 20 s rest, 3 min in total). Following centrifugation (15000 rpm, 4 °C, 30 min). Recombinant proteins were purified using HisPur Ni-NTA Resin (Thermo Scientific). Proteins were eluted with the elution buffer (20 mM Tri-HCl, pH 8, 200 mM NaCl, and 300 mM imidazole). Purified proteins were desalted with a PD-10 column in the storage buffer (25 mM Tris-HCl, pH 8, and 15% glycerol). Protein concentrations were determined by Nanodrop, and protein purity was assessed in SDS-PAGE analysis.

Substrate Selectivity of the Recombinant Adenylation (A) Domains. The reaction mixture (100 μL) contained 25 mM Tris-HCl, pH 8, 15 mM $MgCl_2$, 2.25 mM ATP, 150 mM hydroxylamine, 3 mM amino acid substrate, and 5 μM purified A domain. The tested substrates include L-Ala, L-Gly, L-Ile, L-Leu, L-Pro, L-Tyr and L-Val. The reaction with boiled enzyme was used as the negative control for each reaction. The reactions were incubated in 96-well plates at 30 °C for 15 min and quenched by adding 100 μL stopping solution containing 10% (*w*/*v*) $FeCl_3$, 3.3% (*v*/*v*) trifluoroacetic acid, and 0.7 M HCl. The absorbance at 540 nm of each reaction was recorded on a BioTek multimode microplate reader (Agilent). The absorbance for the negative control was subtracted to calculate the absolute absorbance for each reaction. Each reaction was repeated at least four times, and data was reported as mean ± standard deviations (s.d.).

Synthesis Procedures. *Dipeptide 17.* To a stirred solution of Boc-*N*-methyl-L-isoleucine (**8**) (1g, 4.10 mmol, 1.0 equiv) and sodium bicarbonate (514 mg, 6.15 mmol, 1.5 equiv) in anhydrous DMF (20 mL) was added benzyl bromide (973 μL, 8.19 mmol, 2.0 equiv) at 0 °C. After being stirred at 0 °C to room temperature for 16 h, the reaction mixture was quenched with H_2O and the aqueous layer was extracted with EtOAc. The combined organic layers were washed with brine, dried over $MgSO_4$, filtered, and concentrated in vacuo.

https://doi.org/10.1021/acs.jnatprod.5c00963
J. Nat. Prod. 2025, 88, 2610−2624

The residue was purified by silica gel column chromatography (0−15% EtOAc in hexanes) to give Boc-*N*-methyl-L-isoleucine benzyl ester (810 mg, 59%), which was then dried in vacuo for 30 min. A portion of the compound (499.6 mg, 1.49 mmol, 1.0 equiv) was then resuspended in CH_2Cl_2 (4 mL) and TFA (1.5 mL) was added at 0 °C. After being stirred at 0 °C to room temperature for 1 h, the reaction mixture was coevaporated with toluene three times and concentrated in vacuo to give the crude deprotected amine as a yellow oil, which was used for the next reaction without further purification.

To a stirred solution of the previous deprotected amine in CH_2Cl_2 (10 mL) were added Boc-*N*-methyl-L-leucine (**9**) (365.4 mg, 1.49 mmol, 1.0 equiv), HATU (849.5 mg, 2.23 mmol, 1.5 equiv), and DIEA (778.3 μL, 4.47 mmol, 3.0 equiv) at 0 °C. After being stirred at 0 °C to room temperature for 16 h, the reaction mixture was concentrated in vacuo and diluted with EtOAc. The whole mixture was washed with brine, dried over $MgSO_4$, filtered, and concentrated in vacuo. The residue was purified by silica gel column chromatography (2−20% EtOAc in hexanes) to give **17** (569.5 mg, 83% over two steps) as a colorless oil: $[\alpha]^{26}_D$ −121 (*c* 0.82, MeOH); ^{1}H NMR (600 MHz, $CDCl_3$, a mixture of rotamers) δ 7.33 (m, 5H), 5.18 (dd, *J* = 12.1, 2.6 Hz, 1H), 5.13−5.00 (m, 3H), 4.82 (m, 1H), 2.92 (s, 3H), 2.75 (s, 3H), 2.50 (d, *J* = 7.4 Hz, 1H), 1.59−2.03 (m, 2H), 1.45 (s, 9H), 1.03−1.32 (m, 2H), 0.91 (m, 9H), 0.84 (m, 2H); ^{13}C NMR (150 MHz, $CDCl_3$, a mixture of rotamers, only major reported) δ 172.6 (C), 171.8 (C), 156.0 (C), 135.6 (C), 128.9 (CH x 2), 127.6 (CH), 127.1 (CH x 2), 79.8 (C), 75.7 (CH), 66.4 (CH_2), 62.7 (CH), 37.3 (CH_2), 33.8 (CH), 32.5 (CH_3), 31.3 (CH_3), 28.4 (CH_3 x 3), 25.4 (CH_2), 24.7 (CH), 22.5 (CH_3 x 2), 15.3 (CH_3), 11.3 (CH_3); HRMS (ESI) *m*/*z* 485.2971 $[M + Na]^+$ (calcd for $C_{26}H_{42}N_2O_5Na$, 485.2991).

Tripeptide ***6***. To a stirred solution of dipeptide **17** (435.8 mg, 0.942 mmol, 1.0 equiv) in CH_2Cl_2 (3 mL) were added TFA (1.2 mL) at 0 °C. After being stirred at 0 °C to room temperature for 1 h, the reaction mixture was coevaporated with toluene three times and concentrated in vacuo to give the crude deprotected amine as a yellow oil, which was used for the next reaction without further purification.

To a stirred solution of the previous deprotected amine in CH_2Cl_2 (7 mL) were added Fmoc-*N*,*O*-dimethyl-L-tyrosine (**10**) (406.5 mg, 0.942 mmol, 1.0 equiv), BEP (387 mg, 1.41 mmol, 1.5 equiv), and DIEA (492.3 μL, 2.83 mmol, 3.0 equiv) at 0 °C. After being stirred at 0 °C to room temperature for 16 h, the reaction mixture was concentrated in vacuo and diluted with EtOAc. The whole mixture was washed with brine, dried over $MgSO_4$, filtered, and concentrated in vacuo. The residue was purified by silica gel column chromatography (5−30% EtOAc in hexanes) to give **6** (371 mg, 51% over two steps) as a colorless amorphous solid: $[\alpha]^{26}_D$ −126 (*c* 0.64, MeOH); ^{1}H NMR (600 MHz, $CDCl_3$, a mixture of rotamers, only major reported) δ 7.90 (2H), 7.55 (2H), 7.38 (2H), 7.33 (3H), 7.32 (1H), 7.28 (2H), 7.13 (2H), 6.86 (2H), 5.34−4.70 (2H, m, *J* = 14.5 Hz), 4.92 (1H, dd, *J* = 8.0, 2.9 Hz), 4.46 (1H, d, *J* = 11.2 Hz), 4.44 (1H), 4.23 (1H), 3.81 (3H, s), 3.44−3.19 (2H, m), 3.27 (3H, s), 3.00 (3H, s, H-16), 2.90 (3H, s, H-23), 2.81 (1H, dd, *J* = 13.1, 5.2 Hz), 1.76−1.55 (2H, m), 1.49 (1H, m), 1.11 (3H, s), 0.99 (3H, t), 0.90 (6H, d, *J* = 6.5 Hz); ^{13}C NMR (150 MHz, $CDCl_3$, a mixture of rotamers, only major reported) δ 172.8 (C), 171.5 (C), 170.0 (C), 157.8 (C), 154.3 (C), 143.6 (C x 2), 142.6 (C x 2), 136.1 (C), 129.8 (CH x 2), 128.9 (CH x 2), 128.9 (C), 127.6 (CH), 127.6 (CH x 2), 127.1 (CH x 2), 126.7 (CH x 2), 126.2 (CH x 2), 125.2 (CH x 2), 120.5 (CH x 2), 114.2 (CH x 2), 75.7 (CH), 67.6 (CH_2), 66.4 (CH_2), 63.5 (CH), 61.2 (CH), 55.8 (CH_3), 47.0 (CH), 35.1 (CH_2), 33.8 (CH), 32.5 (CH_3), 31.8 (CH_3), 31.3 (CH_3), 25.4 (CH_2), 24.7 (CH), 22.5 (CH_3 x 2), 15.3 (CH_3), 11.3 (CH_3); HRMS (ESI) *m*/*z* 798.4095 $[M + Na]^+$ (calcd for $C_{47}H_{57}N_3O_7Na$, 798.4094).

Tetrapeptide ***4***. To a stirred solution of tripeptide **6** (41.5 mg) in MeOH (2 mL), Pd/C (6.23 mg) was added at room temperature. After being vigorously stirred under a hydrogen gas atmosphere (balloon pressure) at the same temperature for 1.5 h, the reaction mixture was filtered through a Celite pad, and the filtrate was concentrated in vacuo. The resultant deprotected product was used for the next reaction without further purification (yield = 84.5%).

To a stirred solution of the previous deprotected carboxylic acid (31 mg, 0.0452 mmol, 1.0 equiv) in CH_2Cl_2 (5 mL) were added thiazole **7** (8.37 mg, 0.0542 mmol, 1.2 equiv), BEP (18.6 mg, 0.0678 mmol, 1.5 equiv), and DIEA (23.6 μL, 0.136 mmol, 3.0 equiv) at 0 °C. After being stirred at 0 °C to room temperature for 16 h, the reaction mixture was concentrated in vacuo and diluted with EtOAc. The whole mixture was washed with brine, dried over $MgSO_4$, filtered, and concentrated in vacuo. The residue was purified by silica gel column chromatography (30−70% EtOAc in hexanes) to give **4** (19.1 mg, 43% over two steps) as a colorless amorphous solid: $[\alpha]^{26}_D$ −269 (*c* 0.24, MeOH); ^{1}H NMR (600 MHz, $CDCl_3$, a mixture of rotamers) δ 7.90 (2H), 7.67, (1H), 7.55 (2H), 7.38 (2H), 7.33 (3H), 7.28 (2H), 7.20 (1H), 7.13 (2H), 6.86 (2H), 4.92 (1H, dd, *J* = 8.0, 2.9 Hz), 4.74 (1H), 4.70 (2H), 4.46 (1H, d, *J* = 11.2 Hz), 4.44 (1H), 4.34 (1H), 3.81 (3H, s), 3.51−3.41 (2H, m), 3.44−3.19 (2H, m), 3.27 (3H, s), 3.00 (3H, s), 2.90 (3H, s), 2.48 (1H, dd, *J* = 13.1, 5.2 Hz), 2.38−2.14 (2H, m), 2.02−1.92 (2H, m), 1.76−1.55 (2H, m), 1.11 (3H, s), 0.99 (3H, t), 0.90 (6H, d, *J* = 6.5 Hz); ^{13}C NMR (150 MHz, $CDCl_3$, a mixture of rotamers, only major reported) δ 172.8 (C), 172.6 (C), 170.7 (C), 170.0 (C), 157.8 (C), 154.3 (C), 143.6 (C x 2), 142.6 (C x 2), 141.9 (CH), 129.8 (CH x 2), 128.9 (C), 126.7 (CH x 2), 126.2 (CH x 2), 125.2 (CH x 2), 120.5 (CH x 2), 118.7 (CH), 114.2 (CH x 2), 67.6 (CH_2), 65.9 (CH_2), 64.0 (CH), 63.5 (CH), 60.8 (CH), 55.8 (CH_3), 48.8 (CH_2), 47.0 (CH), 40.5 (CH_2), 35.1 (CH_2), 33.3 (CH), 32.6−24.9 (CH_2), 32.1 (CH_3), 31.8 (CH_3), 31.3 (CH_3), 25.0(CH_2), 24.7 (CH), 22.5 (CH_3 x 2), 14.9 (CH_3); HRMS (ESI) *m*/*z* 822.4242 $[M + H]^+$ (calcd for $C_{47}H_{60}N_5O_6S$, 822.4264).

*5-Desmethyl-lyngbyapeptin A (****2****)*. To a stirred solution of tetrapeptide **4** (13.2 mg, 0.0161 mmol, 1.0 equiv) in MeCN (1.5 mL) was added Et_2NH (0.8 mL) at 0 °C. After being stirred at 0 °C to room temperature for 1 h, the reaction mixture was coevaporated with toluene three times and concentrated in vacuo to give the crude deprotected amine as a colorless oil, which was used for the next reaction without further purification.

To a stirred solution of the previous deprotected amine in CH_2Cl_2 (5 mL) were added excess acetoacetic acid (**5b**), BEP (6.60 mg, 0.0241 mmol, 1.5 equiv), and DIEA (8.39 μL, 0.0482 mmol, 3.0 equiv) at 0 °C. After being stirred at 0 °C to room temperature for 16 h, the reaction mixture was concentrated in vacuo and diluted with EtOAc. The whole mixture was washed with brine, dried over $MgSO_4$, filtered, and concentrated in vacuo. The residue was subsequently purified by normal phase preparative TLC (95:5 CH_2Cl_2-MeOH) and reversed-phase HPLC (Phenomenex; Luna C18(2) 250 × 10 mm, column 250 × 10 mm, 5 μm; flow rate, 2.0 mL/min) using a 69% isocratic method (A: H_2O, B: MeOH; 42 min) to give **2** (5.8 mg, 53% over two steps) as a colorless amorphous solid: $[\alpha]^{26}_D$ −98 (*c* 0.06, MeOH); ^{1}H NMR (600 MHz, $CDCl_3$) δ 7.68 (d, *J* = 3.1 Hz, 1H), 7.22 (d, *J* = 3.1 Hz, 1H), 7.16 (d, *J* = 8.6 Hz, 1H), 6.76 (d, *J* = 8.6 Hz, 1H), 5.76 (dd, *J* = 9.0, 6.2 Hz, 1H), 5.45 (m, 2H), 5.00 (d, *J* = 11.2 Hz, 1H), 3.75−3.96 (m, 2H), 3.74 (s, 3H), 3.52 (d, *J* = 7.0 Hz, 1H), 3.23 (dd, *J* = 13.5, 9.2 Hz, 1H), 2.94 (s, 3H), 2.85 (s, 3H), 2.80 (s, 1H), 2.75 (dd, *J* = 13.5, 6.1 Hz, 1H), 2.67 (s, 3H), 2.20−2.36 (m, 2H), 2.18 (s, 3H), 1.50−1.68 (m, 2H), 1.90−2.03 (m, 3H), 1.25 (s, 1H), 0.94 (3H, d, *J* = 2.7 Hz, H-21), 0.93 (d, *J* = 2.6 Hz, 3H), 0.83 (3H, d, *J* = 6.6 Hz, H-29), 0.76 (3H, m, H-28); ^{13}C NMR (150 MHz, $CDCl_3$) δ 171.4 (C, C-35), 171.1 (C, C-18), 169.6 (C, C-2), 169.0 (C, C-25), 166.8 (C, C-7), 158.6 (C, C-12), 141.1 (CH, C-36), 130.7 (CH, C-10, C-14), 129.8 (C, C-9), 119.0 (CH, C-37), 114.0 (CH, C-11, C-13), 89.8 (CH, C-3), 59.9 (CH, C-31), 58.3 (CH, C-24), 54.5 (CH_3, C-15), 54.4 (CH, C-6), 50.7 (CH, C-17), 47.5 (CH_2, C-34), 37.9 (CH_2, C-19), 34.6 (CH_2, C-8), 31.8 (CH_2, C-32), 31.1 (CH_3, C-16), 30.3 (CH_3, C-30), 30.0 (CH_3, C-23), 24.5 (CH, C-20), 24.3 (CH_2, C-33), 23.3 (CH_3, C-22), 23.5 (CH_2, C-27), 22.1 (CH_3, C-21), 19.1 (CH_3, C-1), 15.1 (CH_3, C-29), 10.4 (CH_3, C-28); HRMS (ESI) *m*/*z* $[M + H]^+$ 684.3784 (calcd for $C_{36}H_{54}N_5O_6S$, 684.3795).

Acrylamide Analogue ***3***. To a stirred solution of the deprotected amine of tetrapeptide **4** (7.9 mg) in CH_2Cl_2 (1 mL) were added excess acrylic acid (**5c**), BEP (5.4 mg, 0.0199 mmol, 1.5 equiv), and DIEA (6.93 μL, 0.0397 mmol, 3.0 equiv) at 0 °C. After being stirred

https://doi.org/10.1021/acs.jnatprod.5c00963
J. Nat. Prod. 2025, 88, 2610−2624

at 0 °C to room temperature for 16 h, the reaction mixture was concentrated in vacuo and diluted with EtOAc. The whole mixture was washed with brine, dried over $MgSO_4$, filtered, and concentrated in vacuo. The residue was subsequently purified by normal phase preparative TLC (95:5 CH_2Cl_2-MeOH) and reversed-phase HPLC (Phenomenex; Luna C18(2) 250 × 10 mm, column 250 × 10 mm, 5 μm; flow rate, 2.0 mL/min) using a 69% isocratic method (A: H_2O, B: MeOH; 42 min) to give **3** (5.8 mg, 65% over two steps) as a colorless amorphous solid: $[\alpha]^{26}_D$ −98 (*c* 0.06, MeOH); ^{1}H NMR (600 MHz, $CDCl_3$) δ 7.68 (d, *J* = 3.1 Hz, 1H), 7.22 (d, *J* = 3.1 Hz, 1H), 7.16 (d, *J* = 8.6 Hz, 1H), 6.76 (d, *J* = 8.6 Hz, 1H), 5.76 (dd, *J* = 9.0, 6.2 Hz, 1H), 5.45 (m, 2H), 5.00 (d, *J* = 11.2 Hz, 1H), 3.75−3.96 (m, 2H), 3.74 (s, 3H), 3.52 (d, *J* = 7.0 Hz, 1H), 3.23 (dd, *J* = 13.5, 9.2 Hz, 1H), 2.94 (s, 3H), 2.85 (s, 3H), 2.80 (s, 1H), 2.75 (dd, *J* = 13.5, 6.1 Hz, 1H), 2.67 (s, 3H), 2.20−2.36 (m, 2H), 2.18 (s, 3H), 1.50−1.68 (m, 2H), 1.90−2.03 (m, 3H), 1.25 (s, 1H), 0.94 (3H, d, *J* = 2.7 Hz, H-21), 0.93 (d, *J* = 2.6 Hz, 3H), 0.83 (3H, d, *J* = 6.6 Hz, H-29), 0.76 (3H, m, H-28); ^{13}C NMR (150 MHz, $CDCl_3$) δ 171.4 (C, C-35), 171.1 (C, C-18), 169.6 (C, C-2), 169.0 (C, C-25), 166.8 (C, C-7), 158.6 (C, C-12), 141.1 (CH, C-36), 130.7 (CH, C-10, C-14), 129.8 (C, C-9), 119.0 (CH, C-37), 114.0 (CH, C-11, C-13), 89.8 (CH, C-3), 59.9 (CH, C-31), 58.3 (CH, C-24), 54.5 (CH_3, C-15), 54.4 (CH, C-6), 50.7 (CH, C-17), 47.5 (CH_2, C-34), 37.9 (CH_2, C-19), 34.6 (CH_2, C-8), 31.8 (CH_2, C-32), 31.1 (CH_3, C-16), 30.3 (CH_3, C-30), 30.0 (CH_3, C-23), 24.5 (CH, C-20), 24.3 (CH_2, C-33), 23.5 (CH_2, C-27), 23.3 (CH_3, C-22), 22.1 (CH_3, C-21), 19.1 (CH_3, C-1), 15.1 (CH_3, C-29), 10.4 (CH_3, C-28); HRMS (ESI) *m*/*z* [M + H]$^+$ 654.3784 (calcd for $C_{35}H_{51}N_5O_5S$, 654.3795).

*Lyngbyapeptin A (**1**). Method 1.* To a stirred solution of 5-desmethyl-lyngbyapeptin A (**2**) (10.8 mg, 0.0158 mmol, 1.0 equiv) in a mixture of Et_2O (2 mL) and MeOH (0.5 mL) at 0 °C was added $TMSCHN_2$ (11.7 μL, 0.0790 mmol, 5 equiv) and DIEA (13.8 μL, 0.0790 mmol, 5 equiv). The resulting mixture was stirred for 24 h at room temperature, then concentrated in vacuo. The residue was purified by normal-phase preparative TLC (95:5 CH_2Cl_2-MeOH) to give unreacted **2** (7.7 mg) and **1** (0.79 mg, 25%) as a colorless amorphous solid.

Method 2. To a stirred solution of the deprotected amine of tetrapeptide **4** (13.2 mg) in CH_2Cl_2 (5 mL) were added excess (*E*)-3-methoxy-2-butenoic acid (**5a**), BEP (6.60 mg, 0.0241 mmol, 1.5 equiv), and DIEA (8.39 μL, 0.0482 mmol, 3.0 equiv) at 0 °C. After being stirred at 0 °C to room temperature for 16 h, the reaction mixture was concentrated in vacuo and diluted with EtOAc. The whole mixture was washed with brine, dried over $MgSO_4$, filtered, and concentrated in vacuo. The residue was subsequently purified by normal phase preparative TLC (7:3 EtOAc-hexanes) and reversed-phase HPLC (Phenomenex; Luna C18(2) 250 × 10 mm, column 250 × 10 mm, 5 μm; flow rate, 2.0 mL/min) using a 61% isocratic method (A: H_2O, B: MeCN; 41 min) to give **1** (3.92 mg, 35% over two steps) as a colorless amorphous solid: $[\alpha]^{26}_D$ −258 (*c* 0.58, MeOH); ^{1}H NMR (600 MHz, $CDCl_3$) δ 7.67 (1H, d, *J* = 3.3 Hz, H-36), 7.21 (1H, d, *J* = 3.3 Hz, H-37), 7.20 (2H, d, *J* = 8.6 Hz, H-10, H-14), 6.75 (2H, d, *J* = 8.6 Hz, H-11, H-13), 5.82 (1H, dd, *J* = 9.7, 5.3 Hz, H-6), 5.45 (1H, dd, *J* = 9.1, 5.8 Hz, H-17), 5.43 (1H, dd, *J* = 8.0, 2.9 Hz, H-31), 5.16 (1H, s, H-3), 4.97 (1H, d, *J* = 11.2 Hz, H-24), 3.94−3.74 (2H, m, H-34), 3.73 (3H, s, H-15), 3.63 (3H, s, H-5), 3.26 (1H, dd, *J* = 13.1, 9.5 Hz, H-8a), 3.00 (3H, s, H-16), 2.80 (3H, s, H-23), 2.70 (1H, dd, *J* = 13.1, 5.2 Hz, H-8b), 2.59 (3H, s, H-30), 2.32−2.21 (2H, m, H-32), 2.20 (3H, s, H-1), 2.14−1.98 (2H, m, H-33), 1.93 (1H, m, H-26), 1.60 (1H, dd, *J* = 13.1, 5.2 Hz, H-19a), 1.54 (1H, dd, *J* = 13.1, 5.2 Hz, H-19b), 1.33 (1H, m, H-20), 0.94 (3H, d, *J* = 6.5 Hz, H-21), 0.92 (3H, d, *J* = 6.7 Hz, H-22), 0.83 (3H, d, *J* = 6.6 Hz, H-29), 0.76 (3H, m, H-28); ^{13}C NMR (150 MHz, $CDCl_3$) δ 171.8 (C, C-35), 171.3 (C, C-18), 170.4 (C, C-2), 170.0 (C, C-25), 169.8 (C, C-7), 168.0 (C, C-4), 158.4 (C, C-12), 142.3 (CH, C-36), 130.7 (CH, C-10, C-14), 129.5 (C, C-9), 118.9 (CH, C-37), 113.8 (CH, C-11, C-13), 90.7 (CH, C-3), 58.6 (CH, C-31), 58.1 (CH, C-24), 55.4 (CH_3, C-15), 55.2 (CH_3, C-5), 54.4 (CH, C-6), 51.7 (CH, C-17), 47.5 (CH_2, C-34), 38.1 (CH_2, C-19), 34.8 (CH_2, C-8), 33.6 (CH, C-26), 31.8 (CH_2, C-32), 31.1 (CH_3, C-16), 30.4 (CH_3, C-30), 30.1 (CH_3, C-23), 24.6 (CH, C-20), 24.5 (CH_2, C-33), 23.5 (CH_2, C-22), 23.5 (CH_2, C-27), 22.5 (CH_3, C-21), 19.1 (CH_3, C-1), 15.1 (CH_3, C-29), 10.4 (CH_3, C-28); HRMS (ESI) *m*/*z* 720.3755 [M + Na]$^+$ (calcd for $C_{37}H_{55}N_5O_6SNa$, 720.3771).

Functional GPCR Target-Based Profiling Using β-Arrestin Assays. Lyngbyapeptin A (**1**) and analogue **2** (20 μM each) were individually profiled against gpcrMAX panel biosensor assays (in agonist and antagonist modes) against a panel of 168 GPCRs. The assays were performed by DiscoverX Corporation (Fremont, CA) using enzyme fragment complementation (EFC) technology. The PathHunter cell lines were expanded from freezer stocks according to standard procedures. Cells were seeded in a total volume of 20 μL into white-walled, 384-well microplates and incubated at 37 °C for the appropriate time prior to testing.

For agonist determination, both compounds were incubated with PathHunter cell lines to induce response. Intermediate dilution of sample stocks was performed to generate 5x sample in assay buffer. Then, 5 μL of 5x sample was added to cells and incubated at 37 °C or room temperature for 90 or 180 min. Final assay vehicle concentration was 1%.

For antagonist determination, PathHunter cells were preincubated with both compounds followed by the addition of an agonist at the EC_{80} concentration. Intermediate dilution of sample stocks was performed to generate 5x sample in assay buffer. Then, 5 μL of 5x sample was added to cells and incubated at 37 °C or room temperature for 30 min. Vehicle concentration was 1%. After that, 5 μL of 6x EC_{80} agonist in assay buffer was added to the cells and incubated at 37 °C or room temperature for 90 or 180 min.

Assay signal was generated through a single addition of 12.5 or 15 μL (50% v/v) of PathHunter Detection reagent cocktail, followed by 1 h incubation at room temperature. Microplates were read following signal generation with a PerkinElmer Envision instrument for chemiluminescent signal detection. Compound activity was analyzed using CBIS data analysis suite (ChemInnovation, CA).

Hit validation was performed by subjecting lyngbyapeptin A (**1**), 5-desmethyl-lyngbyapeptin A (**2**), and acrylamide analogue **3** to antagonist secondary screen utilizing four GPCR biosensor assays (Arrestin) against the following targets: CALCR-RAMP2, CNR1, CNR2, and MLNR. The assays were performed at 10-point concentrations using 3-fold serial dilutions in duplicate.

Calcium Flux Assay. The assay in antagonist format was performed by DiscoverX Corporation (Fremont, CA). Human MLNR in stably transfected CHO-K1 cells were seeded in a total volume of 20 μL into black-walled, clear-bottom, Poly-D-lysine coated microplates and incubated at 37 °C. Prior to testing, media was exchanged with 20 μL of Dye Loading Buffer (1x Dye, 1x Additive A and 2.5 mM Probenecid in HBSS/20 mM Hepes), then incubated for 30−60 min at 37 °C. Intermediate dilution of sample stocks was performed to generate 3x sample in assay buffer. After dye loading, 10 μL of 3x sample was added to cells and incubated in the dark at room temperature for 30 min to equilibrate plate temperature. Vehicle concentration was 1%. Compound antagonist activity was measured on a FLIPR Tetra (MDS). Calcium mobilization was monitored for 2 min and 10 μL of EC_{80} motilin in HBSS/20 mM Hepes was added to the cells 5 s into the assay. Compound activity was analyzed using CBIS data analysis suite (ChemInnovation, CA). The assays were performed at 10-point concentrations of **1** using 3-fold serial dilutions in duplicate, where the highest concentration was 100 μM.

Motilin Receptor MLNR Binding Assay. The assay was carried out by Eurofins Panlabs Discovery Services (New Taipei City, Taiwan). Human recombinant motilin receptors expressed in human embryonic kidney HEK293 cells were used in modified Tris buffer (50 mM Tris, pH 7.4, 10 mM $MgCl_2$, 0.5% BSA). An aliquot of membrane homogenate was incubated with 0.1 nM [^{125}I]motilin for 2.5 h at 25 °C. Nonspecific binding was estimated in the presence of 1 μM motilin. Membranes were filtered and washed four times and the filters were counted to determine [^{125}I]motilin as specifically bound. Compound **1** was screened at 8 concentrations, where the highest concentration was 100 μM. All compounds were dissolved in DMSO

https://doi.org/10.1021/acs.jnatprod.5c00963
J. Nat. Prod. 2025, 88, 2610−2624

to give a final concentration of 1% DMSO. The experiments were carried out as technical duplicates.

Cannabinoid CNR1 Receptor Binding Assay. The assay was carried out by Eurofins Panlabs Discovery Services (New Taipei City, Taiwan). Human recombinant cannabinoid CNR1 receptors expressed in rat hematopoietic Chem-1 cells were used in modified HEPES buffer (50 mM HEPES, pH 7.4, 5 mM $MgCl_2$, 1 mM $CaCl_2$, 0.2% BSA). A 5 μg aliquot of membrane homogenate was incubated with 2 nM [^{3}H]SR141716A for 60 min at 37 °C. Nonspecific binding was estimated in the presence of 10 μM CP 55,940. Membranes were filtered and washed four times and the filters were counted to determine [^{3}H]SR141716A as specifically bound. Compound **1** was screened at 8 concentrations, where the highest concentration was 100 μM. All compounds were dissolved in DMSO to give a final concentration of 1% DMSO. The experiments were carried out as technical duplicates.

Molecular Docking with MLNR. The model for MLNR was obtained from the cryo-EM structure of MLNR in complex with erythromycin at 3.5 Å resolution (PDBID: 8IBU).[42] The structure was prepared using Schrödinger Protein Preparation Workflow at pH 7.4 ± 1.0. The ligand lyngbyapeptin A (**1**) was drawn using Maestro 2D sketcher and prepared with Schrödinger LigPrep. Compound **1** was docked into MLNR binding site with Schrödinger GlideSP,[54] and the bound structure with the lowest Glide Docking Score and Glide Emodel scores was selected for molecular dynamics simulations.

Molecular Dynamics with MLNR. MD simulations were carried out with Schrödinger Desmond MD engine. The systems were embedded in a POPC membrane, which was included in an orthorhombic box with SPC waters. Counterions were added to neutralize the charges, and extra ion pairs were added to reach a salt concentration of 0.15 M. The OPLS4 force field was used for all atoms except water. The simulations used the NPγT ensemble at 1 atm pressure and 300 K. Membrane models were relaxed with Schrödinger standard membrane relaxation protocol and simulations were run for 100 ns.

Molecular Docking with CNR1. The model for CNR1 was obtained from the crystal structure of CNR1 in complex with AM6538 at 2.8 Å resolution (PDBID: 5TGZ).[55] The structure was prepared using Schrödinger Protein Preparation Workflow at pH 7.4 ± 1.0. The ligand **1** was drawn using Maestro 2D sketcher and prepared with Schrödinger LigPrep. Compound **1** was docked into CNR1 binding site with Schrödinger GlideSP,[54] and the bound structure with the lowest Glide Docking Score and Glide Emodel scores was selected for molecular dynamics simulations.

Molecular Dynamics with CNR1. MD simulations were carried out with Schrödinger Desmond MD engine. The systems were embedded in a POPC membrane, which was included in an orthorhombic box with SPC waters. Counterions were added to neutralize the charges, and extra ion pairs were added to reach a salt concentration of 0.15 M. The OPLS4 force field was used for all atoms except water. The simulations used the NPγT ensemble at 1 atm pressure and 310 K. Membrane models were relaxed with Schrödinger standard membrane relaxation protocol and simulations were run for 100 ns.

MTT Cell Viability Assay. Human colorectal carcinoma cells HCT116 (ATCC) and human embryonic kidney cells HEK293 transfected with Nrf2/ARE responsive luciferase reporter gene (HEK293-ARE-luc) (SL-0042-NP; Signosis) were propagated and maintained using Dulbecco's Modified Eagle's Medium (DMEM; Invitrogen, Waltham, MA, USA) supplemented with 10% fetal bovine serum (FBS; Sigma, St. Louis, MO, USA), and 1% antibiotic-antimycotic (Invitrogen) at 37 °C humidified air and 5% CO_2. Cells were seeded at a density of 10,000 cells per well in 96-well plates. Wells with negative control (cells + medium +0.1% DMSO) and medium only (media +0.1% DMSO) were also incorporated to establish maximum viability and background absorbance. After 16 h of incubation, the cells were treated with varying concentrations of compounds **1**−**3** or DMSO. Cells were then incubated with compounds for 48 h, followed by addition of the MTT reagent (Promega). Cell viability was measured according to the manufacturer's instructions, recorded on a SpectraMax M5, and the subsequent data were processed via GraphPad Prism 6.

ARE-Luciferase Assay. HEK293-ARE-luc cells (10,000 cells per well) were seeded in 96-well format in white solid plates. After 16 h of incubation, the cells were treated with varying concentrations of compounds **1**−**3**, 10 μM of *tert*-butylhydroquinone (TBHQ) as positive control, or DMSO. Luciferase activity was detected at 24 h post-treatment using BriteLite detection reagent (PerkinElmer) following the manufacturer's protocol, and luminescence was read with an Envision (PerkinElmer) plate reader. A complementary MTT cell viability assay was performed along with the reporter assay as described above.

■ ASSOCIATED CONTENT

Data Availability Statement

All data supporting the findings of this study are available within the article and its Supporting Information. The sequence of *lynA* BGC was deposited at NCBI under Project NCBI accession PV754024.

Supporting Information

The Supporting Information is available free of charge at https://pubs.acs.org/doi/10.1021/acs.jnatprod.5c00963.

Bioinformatic analysis of biosynthetic genes and biochemical studies (Tables S1−S4 and Figure S1); bioassay data (Figures S2 and S10); computational data (Figures S3−S9); ^{1}H NMR comparison of isolated and published **1** (Figure S11); NMR spectra of new synthetic compounds and comparison of synthetic and isolated **1** (Figures S12−S26) (PDF)

■ AUTHOR INFORMATION

Corresponding Author

Hendrik Luesch − *Department of Medicinal Chemistry, University of Florida, Gainesville, Florida 32610, United States; Center for Natural Products, Drug Discovery and Development (CNPD3), University of Florida, Gainesville, Florida 32610, United States; Program in Cancer and Stem Cell Biology, Duke-NUS Medical School, Singapore 169857, Singapore;* orcid.org/0000-0002-4091-7492; Email: luesch@cop.ufl.edu

Authors

Tam H. D. Pham − *Department of Medicinal Chemistry, University of Florida, Gainesville, Florida 32610, United States; Center for Natural Products, Drug Discovery and Development (CNPD3), University of Florida, Gainesville, Florida 32610, United States*

Manyun Chen − *Department of Medicinal Chemistry, University of Florida, Gainesville, Florida 32610, United States; Center for Natural Products, Drug Discovery and Development (CNPD3), University of Florida, Gainesville, Florida 32610, United States;* orcid.org/0000-0001-6803-044X

Jie Liu − *Department of Molecular Biology, Princeton University, Princeton, New Jersey 08544, United States*

Qi-Yin Chen − *Department of Medicinal Chemistry, University of Florida, Gainesville, Florida 32610, United States; Center for Natural Products, Drug Discovery and Development (CNPD3), University of Florida, Gainesville, Florida 32610, United States*

Gustavo Seabra − *Department of Medicinal Chemistry, University of Florida, Gainesville, Florida 32610, United States; Center for Natural Products, Drug Discovery and*

Development (CNPD3), University of Florida, Gainesville, Florida 32610, United States; orcid.org/0000-0002-1303-4483

Valerie J. Paul − *Smithsonian Marine Station, Fort Pierce, Florida 34949, United States;* orcid.org/0000-0002-4691-1569

Mohamed S. Donia − *Department of Molecular Biology, Princeton University, Princeton, New Jersey 08544, United States*

Steven D. Bruner − *Center for Natural Products, Drug Discovery and Development (CNPD3), University of Florida, Gainesville, Florida 32610, United States; Department of Chemistry, University of Florida, Gainesville, Florida 32611, United States;* orcid.org/0000-0002-0522-480X

Yousong Ding − *Department of Medicinal Chemistry, University of Florida, Gainesville, Florida 32610, United States; Center for Natural Products, Drug Discovery and Development (CNPD3), University of Florida, Gainesville, Florida 32610, United States;* orcid.org/0000-0001-8610-0659

Complete contact information is available at: https://pubs.acs.org/10.1021/acs.jnatprod.5c00963

Author Contributions

Designing experiments: T.H.D.P., M.C., J.L., Q.-Y.C., G.S., and H.L.; sample collection: V.J.P.; genome assembly: J.L.; bioinformatic analysis: M.C.; synthesis, ARE-luciferase reporter, and cytotoxicity assays: T.H.D.P.; computational modeling: T.H.D.P. and G.S.; writing-original draft preparation: T.H.D.P.; writing-review and editing: M.C., J.L., Q.-Y.C., G.S., V.J.P., M.S.D., S.D.B., Y.D., and H.L. All authors have read and agreed to the published version of the manuscript.

Notes

The authors declare no competing financial interest.

■ ACKNOWLEDGMENTS

This research was supported by the National Institutes of Health, National Institute of General Medical Sciences grant RM1GM145426. H.L also acknowledges the Debbie and Sylvia DeSantis Chair Professorship. We thank the Guam Department of Agriculture Division of Aquatic and Wildlife Resources for the research permit and the University of Guam Marine Laboratory for hosting our visit.

■ REFERENCES

(1) Yang, D.; Zhou, Q.; Labroska, V.; Qin, S.; Darbalaei, S.; Wu, Y.; Yuliantie, E.; Xie, L.; Tao, H.; Cheng, J.; Liu, Q.; Zhao, S.; Shui, W.; Jiang, Y.; Wang, M.-W. *Signal Transduct Target Ther* **2021**, *6* (1), 7.
(2) Lorente, J. S.; Sokolov, A. V.; Ferguson, G.; Schiöth, H. B.; Hauser, A. S.; Gloriam, D. E. *Nat. Rev. Drug Discov* **2025**, *24* (6), 458−479.
(3) Rehman, S.; Rahimi, N.; Dimri, M. Biochemistry, G Protein Coupled Receptors. *StatPearls*; StatPearls Publishing: Treasure Island, FL, 2025.
(4) Zhang, M.; Chen, T.; Lu, X.; Lan, X.; Chen, Z.; Lu, S. *Signal Transduct Target Ther* **2024**, *9* (1), 88.
(5) Liu, N.; Wang, Y.; Li, T.; Feng, X. *Int. J. Mol. Sci.* **2021**, *22* (10), 5260.
(6) Calebiro, D.; Nikolaev, V. O.; Persani, L.; Lohse, M. J. *Trends Pharmacol. Sci.* **2010**, *31* (5), 221−228.
(7) O'Hayre, M.; Degese, M. S.; Gutkind, J. S. *Curr. Opin Cell Biol.* **2014**, *27*, 126−135.
(8) Jean-Charles, P.-Y.; Kaur, S.; Shenoy, S. K. *J. Cardiovasc Pharmacol* **2017**, *70* (3), 142.
(9) Xie, W.; Lai, J.; Cai, H.; Eric Xu, H.; Yin, W. *Med. Drug Discov* **2024**, *24*, 100201.
(10) Luesch, H.; Ellis, E. K.; Chen, Q.-Y.; Ratnayake, R. *Nat. Prod Rep* **2025**, *42* (2), 208−256.
(11) Tan, L. T.; Salleh, N. F. *Molecules* **2024**, *29* (22), 5307.
(12) El-Seedi, H. R.; El-Mallah, M. F.; Yosri, N.; Alajlani, M.; Zhao, C.; Mehmood, M. A.; Du, M.; Ullah, H.; Daglia, M.; Guo, Z.; Khalifa, S. A. M.; Shou, Q. *Marine Drugs* **2023**, *21* (8), 439.
(13) Tan, L. T.; Phyo, M. Y. *Molecules* **2020**, *25* (9), 2197.
(14) Davenport, A. P.; Scully, C. C. G.; De Graaf, C.; Brown, A. J. H.; Maguire, J. J. *Nat. Rev. Drug Discov* **2020**, *19* (6), 389−413.
(15) Muratspahić, E.; Freissmuth, M.; Gruber, C. W. *Trends Pharmacol. Sci.* **2019**, *40* (5), 309−326.
(16) Al-Awadhi, F. H.; Gao, B.; Rezaei, M. A.; Kwan, J. C.; Li, C.; Ye, T.; Paul, V. J.; Luesch, H. *J. Med. Chem.* **2018**, *61* (14), 6364−6378.
(17) Liang, X.; Luo, D.; Yan, J.-L.; Rezaei, M. A.; Salvador-Reyes, L. A.; Gunasekera, S. P.; Li, C.; Ye, T.; Paul, V. J.; Luesch, H. *Org. Lett.* **2019**, *21* (6), 1622−1626.
(18) Kokkaliari, S.; Grauso, L.; Mangoni, A.; Seabra, G.; Paul, V. J.; Luesch, H. *Chem.—Eur. J.* **2024**, *30* (50), No. e202401393.
(19) Klein, D.; Braekman, J.-C.; Daloze, D.; Hoffmann, L.; Castillo, G.; Demoulin, V. *Tetrahedron Lett.* **1999**, *40* (4), 695−696.
(20) Luesch, H.; Yoshida, W. Y.; Moore, R. E.; Paul, V. J. *J. Nat. Prod* **2000**, *63* (10), 1437−1439.
(21) Luesch, H.; Yoshida, W. Y.; Moore, R. E.; Paul, V. J. *Tetrahedron* **2002**, *58* (39), 7959−7966.
(22) Matthew, S.; Salvador, L. A.; Schupp, P. J.; Paul, V. J.; Luesch, H. *J. Nat. Prod* **2010**, *73* (9), 1544−1552.
(23) Williams, P. G.; Luesch, H.; Yoshida, W. Y.; Moore, R. E.; Paul, V. J. *J. Nat. Prod* **2003**, *66* (5), 595−598.
(24) Kudo, F.; Chikuma, T.; Nambu, M.; Chisuga, T.; Sumimoto, S.; Iwasaki, A.; Suenaga, K.; Miyanaga, A.; Eguchi, T. *ACS Chem. Biol.* **2023**, *18* (4), 875−883.
(25) Luesch, H.; Yoshida, W. Y.; Moore, R. E.; Paul, V. J.; Corbett, T. H. *J. Am. Chem. Soc.* **2001**, *123* (23), 5418−5423.
(26) Luesch, H.; Yoshida, W. Y.; Moore, R. E.; Paul, V. J. *Bioorg. Med. Chem.* **2002**, *10* (6), 1973−1978.
(27) Challis, G. L.; Ravel, J.; Townsend, C. A. *Chem. Biol.* **2000**, *7* (3), 211−224.
(28) Stachelhaus, T.; Mootz, H. D.; Marahiel, M. A. *Chem. Biol.* **1999**, *6* (8), 493−505.
(29) Pan, G.; Xu, Z.; Guo, Z.; null; Ma, M.; Yang, D.; Zhou, H.; Gansemans, Y.; Zhu, X.; Huang, Y.; Zhao, L.-X.; Jiang, Y.; Cheng, J.; Nieuwerburgh, F. Van; Suh, J.-W.; Duan, Y.; Shen, B. *Proc. Natl. Acad. Sci. U. S. A.* **2017**, *114* (52), E11131−E11140.
(30) Hanquet, G.; Salom-Roig, X. J.; Gressot-Kempf, L.; Lanners, S.; Solladié, G. *Tetrahedron Asymmetry* **2003**, *14* (10), 1291−1301.
(31) Owusu-Ansah, E.; Durow, A. C.; Harding, J. R.; Jordan, A. C.; O'Connell, S. J.; Willis, C. L. *Org. Biomol. Chem.* **2011**, *9* (1), 265−272.
(32) Ma, X.; Chen, Y.; Chen, S.; Xu, Z.; Ye, T. *Org. Biomol Chem.* **2017**, *15* (34), 7196−7203.
(33) Valeur, E.; Bradley, M. *Chem. Soc. Rev.* **2009**, *38* (2), 606−631.
(34) Liang, X.; Matthew, S.; Chen, Q.-Y.; Kwan, J. C.; Paul, V. J.; Luesch, H. *Org. Lett.* **2019**, *21* (18), 7274−7278.
(35) Baird, L.; Yamamoto, M. *Mol. Cell. Biol.* **2020**, *40* (13), No. e00099-20.
(36) Bousquet, M. S.; Ratnayake, R.; Pope, J. L.; Chen, Q.-Y.; Zhu, F.; Chen, S.; Carney, T. J.; Gharaibeh, R. Z.; Jobin, C.; Paul, V. J.; Luesch, H. *Free Radic Biol. Med.* **2020**, *146*, 306−323.
(37) Mackie, K. *J. Neuroendocrinol* **2008**, *20* (s1), 10−14.
(38) Svizenska, I.; Dubovy, P.; Sulcova, A. *Pharmacol., Biochem. Behav.* **2008**, *90* (4), 501−511.
(39) Tadijan, A.; Vlašić, I.; Vlainić, J.; Đikić, D.; Oršolić, N.; Jazvinšćak Jembrek, M. *Antioxidants* **2022**, *11* (10), 2049.
(40) An, D.; Peigneur, S.; Hendrickx, L. A.; Tytgat, J. *Int. J. Mol. Sci.* **2020**, *21* (14), 5064.

(41) Sanger, G. J.; Wang, Y.; Hobson, A.; Broad, J. *Br. J. Pharmacol.* **2013**, *170* (7), 1323−1332.
(42) You, C.; Zhang, Y.; Xu, Y.; Xu, P.; Li, Z.; Li, H.; Huang, S.; Chen, Z.; Li, J.; Xu, H. E.; Jiang, Y. *Sci. Adv.* **2023**, *9* (11), No. eade9020.
(43) Sanger, G. J.; Furness, J. B. *Nat. Rev. Gastroenterol Hepatol* **2016**, *13* (1), 38−48.
(44) Kotliar, I. B.; Lorenzen, E.; Schwenk, J. M.; Hay, D. L.; Sakmar, T. P. *Pharmacol Rev.* **2023**, *75* (1), 1−34.
(45) Cao, J.; Belousoff, M. J.; Gerrard, E.; Danev, R.; Fletcher, M. M.; Dal Maso, E.; Schreuder, H.; Lorenz, K.; Evers, A.; Tiwari, G.; Besenius, M.; Li, Z.; Johnson, R. M.; Wootten, D.; Sexton, P. M. *Nat. Chem. Biol.* **2024**, *20* (2), 162−169.
(46) Hay, D. L.; Chen, S.; Lutz, T. A.; Parkes, D. G.; Roth, J. D. *Pharmacol Rev.* **2015**, *67* (3), 564−600.
(47) Masi, L.; Brandi, M. L. *Clin Cases Miner Bone Metab* **2007**, *4* (2), 117−122.
(48) Morar, M.; Pengelly, K.; Koteva, K.; Wright, G. D. *Biochemistry* **2012**, *51* (8), 1740−1751.
(49) Peeters, T.; Matthijs, G.; Depoortere, I.; Cachet, T.; Hoogmartens, J.; Vantrappen, G. *American Journal of Physiology-Gastrointestinal and Liver Physiology* **1989**, *257* (3), G470−G474.
(50) Xu, L.; Depoortere, I.; Vertongen, P.; Waelbroeck, M.; Robberecht, P.; Peeters, T. L. *Biochem. Pharmacol.* **2005**, *70* (6), 879−887.
(51) Assié, M.-B.; Cosi, C.; Koek, W. *Eur. J. Pharmacol.* **1999**, *386* (1), 97−103.
(52) Blin, K.; Shaw, S.; Vader, L.; Szenei, J.; Reitz, Z. L.; Augustijn, H. E.; Cediel-Becerra, J. D. D.; de Crécy-Lagard, V.; Koetsier, R. A.; Williams, S. E.; Cruz-Morales, P.; Wongwas, S.; Segurado Luchsinger, A. E.; Biermann, F.; Korenskaia, A.; Zdouc, M. M.; Meijer, D.; Terlouw, B. R.; van der Hooft, J. J. J.; Ziemert, N.; Helfrich, E. J. N.; Masschelein, J.; Corre, C.; Chevrette, M. G.; van Wezel, G. P.; Medema, M. H.; Weber, T. *Nucleic Acids Res.* **2025**, *53* (W1), W32−W38.
(53) Röttig, M.; Medema, M. H.; Blin, K.; Weber, T.; Rausch, C.; Kohlbacher, O. *Nucleic Acids Res.* **2011**, *39* (suppl_2), W362−W367.
(54) Halgren, T. A.; Murphy, R. B.; Friesner, R. A.; Beard, H. S.; Frye, L. L.; Pollard, W. T.; Banks, J. L. *J. Med. Chem.* **2004**, *47* (7), 1750−1759.
(55) Hua, T.; Vemuri, K.; Pu, M.; Qu, L.; Han, G. W.; Wu, Y.; Zhao, S.; Shui, W.; Li, S.; Korde, A.; Laprairie, R. B.; Stahl, E. L.; Ho, J. H.; Zvonok, N.; Zhou, H.; Kufareva, I.; Wu, B.; Zhao, Q.; Hanson, M. A.; Bohn, L. M.; Makriyannis, A.; Stevens, R. C.; Liu, Z. J. *Cell* **2016**, *167* (3), 750−762.

https://doi.org/10.1021/acs.jnatprod.5c00963
J. Nat. Prod. 2025, 88, 2610−2624